Synthesis and Characterization of Mn-Zn Ferrite Nanomaterials by Chemical Co-precipitation Method

Thesis submitted in partial fulfillment of the requirement for

the award of the degree of

Master of Technology

In

MATERIALS SCIENCE AND ENGINEERING

Submitted by

Ravi Prakash Srivastava

Roll No.60602011

Under

the guidance of

Dr. O.P.Pandey

Prof. & Head,

School of Physics and Material Science

Thapar University, Patiala (Punjab)

School of Physics & Material Sciences

Thapar University, Patiala

Patiala – 147001

June-2008

CERTIFICATE

This is to certify that the thesis work entitled **"Synthesis and Characterization of Mn-Zn Ferrite Nanomaterial by Chemical Coprecipitation Method"** submitted by Mr. Ravi Prakash Srivastava in the partial fulfillment of the requirement of the award of the degree of M.Tech. in Material Science and Engineering from the School of Physics and Material Science, Thapar University, Patiala (Punjab) is a record of candidates own work carried out by him under my supervision and guidance. The matter embodied in this thesis has not been submitted in any part or full to any other university or institute for the award of any degree.

O.P.Pandey
(Dr. O.P.Pandey)
Supervisor

Countersignned by,

O.P.Pandey
Dr. O.P.Pandey
Prof. & Head
SPMS, Thapar University
Patiala (Punjab)

R.K.Sharma
Dr.R.K.Sharma
Dean Academic Affairs
Thapar University
Patiala (Punjab)

Acknowledgement

I visualize a rare movement of pride and pleasure to extend my sincere and heedful gratitude to my Guide ***Dr. O.P.Pandey, Head School of Physics and Material Science*** *in Thapar university Patiala (Punjab) for not only providing me his inspiring and talented guidance but also his constant attention and constructive and healthy criticism throughout the time. I, infact find paucity of words to express his sound knowledge of the subject and keen interest in it and his potential during the course of the work.*

My greatest thanks are to ***Dr. K.K.Raina, Deputy Director Thapar University*** *and* ***Dr. N. K. Verma, Dean Student Affairs Thapar University*** *for their full motivation and appreciation to my work. They provide me moral support as well as necessary help during my experimental work.*

I am highly greatful to ***Dr. Kulvir Singh, Asst. Prof. School Of Physics And Material Science, Thapar University Patiala (Punjab)*** *for their kind help and valuable suggestions and special attention throughout my work. It is due to his moral encouragement, love and providing me fountain of inspiration, all sorts of assistance from time to time into up-bringing me upto this stage.*

I am also indebted to ***Dr. D.P. Singh, Dr.S.D.Tiwari, Dr.Sanjeev Das*** *and all other faculty members in SPMS, Thapar University Patiala (Punjab) for their graceful and kind hearted support. I would like to thank* ***Dr.Sunil Kumar,*** *Research Associate, School of Physics and Materials Science for his kind attention and valuable suggestions during course of my work.*

My special thanks ***Mr. Purushottam.*** *His assistance and partnership were of great pleasure. His comments and views were very insightful and helpful. I would also like to*

thank ***Mr. Jant Singh*** *and* ***Mr. Inder Mani*** *for providing all kind of assistance in PG Lab and department for creating a healthy research environment.*

I would also like to give many thanks to Research Scholars ***Mr. Vishal, Ms. Anu Arora*** *and* ***Ms.Zinki Jindal,*** *for any kind of help and valuable suggestions whenever I needed out of their busy schedule.*

I am very much thankful to my father ***Sri Jagdish Prasad Srivastava,*** *my mother* ***Smt. Krishna Srivastava,*** *my elder brothers* ***Sri Rajni Kant Srivastava*** *and* ***Sri Chandra Bhushan Srivastava*** *who provided me mental and financial support for this Project work. I am also thankful to my younger sisters* ***Nidhi Srivastava*** *and* ***Ruchi Srivastava*** *for providing me mental encouragement at every time of work.*

Date: 01-07-2008

Place: Patiala

Ravi Prakash Srivastava

(Roll.No.-60602011)

Abstract

Mn-Zn ferrite is a soft magnetic material and is widely used in electronic applications. In order to utilise these materials for the application at higher frequencies it is essential that particle size should be small. Further for the better properties of these materials the particles should be uniform and non-agglomerated. In order to achieve these properties many research groups have shifted towards developing these materials at the nanoscale as the performance in their ceramic preparation route is reaching their limits due to their higher electrical conductivity and domain wall resonance. Therefore the synthesis has been done with the help of chemical co-precipitation method so that we can get high purity material with a small particle size. The main focus of the present work is to synthesize the Mn-Zn ferrite from pure chemicals as well as from the waste material (blue dust) which is the natural ore of the iron. The characterization of the materials synthesized from pure chemicals and blue dust has been done with the help of X-ray analysis, EDS, SEM, TEM and DTA techniques. The results shows that the material synthesized from the blue dust has nearly same properties as that from the pure chemicals. Hence in the coming future the synthesis of Mn-Zn ferrite material from the waste material (blue dust) can be helpful in the cost minimization and we can get cheap electonic devices.

List of Figures

List of Tables

List of Abbreviations

XRD	X-Ray Diffraction
EDS	Energy Dispersive Spectroscopy
SEM	Scanning Electron Microscopy
TEM	Transmission Electron Microscopy
DTA	Differential Thermal Analysis

Content

Abstract

Mn-Zn ferrite is a soft magnetic material and is widely used in electronic applications. In order to utilise these materials for the application at higher frequencies it is essential that particle size should be small. Further for the better properties of these materials the particles should be uniform and non-agglomerated. In order to achieve these properties many research groups have shifted towards developing these materials at the nanoscale as the performance in their ceramic preparation route is reaching their limits due to their higher electrical conductivity and domain wall resonance. Therefore the synthesis has been done with the help of chemical co-precipitation method so that we can get high purity material with a small particle size. The main focus of the present work is to synthesize the Mn-Zn ferrite from pure chemicals as well as from the waste material (blue dust) which is the natural ore of the iron. The characterization of the materials synthesized from pure chemicals and blue dust has been done with the help of X-ray analysis, EDS, SEM, TEM and DTA techniques. The results shows that the material synthesized from the blue dust has nearly same properties as that from the pure chemicals. Hence in the coming future the synthesis of Mn-Zn ferrite material from the waste material (blue dust) can be helpful in the cost minimization and we can get cheap electonic devices.

List of Figures

Figure **Page No.**

List of Tables

List of Abbreviations

XRD X-Ray Diffraction

EDS	Energy Dispersive Spectroscopy
SEM	Scanning Electron Microscopy
TEM	Transmission Electron Microscopy
DTA	Differential Thermal Analysis

Content

Page No.

CHAPTER-1
INTRODUCTION

1.1 History

In the recent times, iron and its alloys were used as magnetic materials for the applications in the electrical industry. However, with the discovery of higher frequencies, the customary techniques

to reducing eddy current losses, using lamination or iron powder cores, were no longer efficient or cost effective. This realization stimulated a renewed interest in "magnetic insulators" as first reported by S. Hilpert in Germany in 1909. It was readily understood that if the high electrical resistivity of oxides could be combined with desired magnetic characteristics, a magnetic material would result that was particularly well suited for high frequency operation. These materials are called ferrites which have general formula MFe_3O_4 where M is the divalent ion like Zn^{++}, Mn^{++}.

Research in order to develop this type of material, was undertaken in various laboratories all over the world, such as by V. Kato, T. Takei, and N. Kawai in the 1930's in Japan and by J. Snoek of the Philips Research Laboratories in the period 1935-45 in the Netherlands. By 1945 Snoek had laid down the basic fundamentals of the physics and technology of practical ferrite materials. In 1948, the Neel theory of ferromagnetic provided the theoretical understanding of this type of magnetic material.

These ferrites are ceramic, homogeneous materials composed of various oxides with iron oxide as their main constituent and fall in the category of soft and hard ferrites. Based upon the chemical composition, soft ferrites can be divided into two major categories, manganese-zinc ferrite and nickel-zinc ferrite. In each of these categories many different Mn-Zn and Ni-Zn material grades are being manufactured by varying the chemical composition or by different manufacturing techniques. The two families of Mn-Zn and Ni-Zn ferrite materials complement each other and allow the use of soft ferrites from audio frequencies to several hundred mega-hertz. The first practical soft ferrite application was in inductors used in LC filters in frequency division multiplex equipment. The combination of high resistivity and good magnetic properties made these ferrites an excellent core material for these filters operating over the 50-450 kHz frequency range. The large scale introduction of TV in the 1950's was a major opportunity for the fledgling ferrite industry. In TV sets, ferrite cores were the material of choice for the high voltage transformer and the picture tube deflection system. For four decades ferrite components have been used in an ever widening range of applications and in steadily increasing quantities, a few are mentioned in Table 1.1 below.

Table 1.1 Soft ferrite applications.

Magnetic device	Application
Power transformers and Chokes	High frequency power supplies
Inductors and tuned transformers	Frequency selective circuits
Pulse and wide band transformers	Matching devices
Magnetic deflection structures	TV sets and monitors
Recording heads	Memory storage devices
Rotating transformers	VCR's
Transducers	Vending machines and ultrasonic cleaners

Table 1.2 Merits and demerits of ferrites over other magnetic materials.

Advantages	Disadvantages
High resistivity	Low saturation flux density
Wide range of operating frequencies	Poor thermal conductivity
Low loss combined with high permeability	Low tensile strength
Time and temperature stability	Brittle material
Large material selection	
Versatility of core shapes	
Low cost	
High resistivity	

These cubic ferrites are especially useful due to two key characteristics :

- High magnetic permeability, which concentrates and enhances the magnetic field.

- High electrical resistivity, which ensures total penetration of the electromagnetic (EM) field.

Furthermore, the dominance of ferrites rests upon a remarkable flexibility in providing tailor-made solutions, ease of preparation, and price and performance considerations. Hence ferrites are widely manufactured into circuit elements, like inductors and cores, reading-writing heads and information storage media.

Amongst the soft ferrites, Manganese Zinc Ferrites are most common, and are used in many more applications than their counterparts, such as nickel-zinc ferrites. Within the Mn-Zn category, large varieties of materials are possible, and the material selection is mainly a function of the application that needs to be accommodated. The application dictates the desirable material characteristics, which in turn determines the chemical composition of the ferrite material. Manganese zinc ferrites are primarily used for frequencies less than 2 MHz. Figure-1 shows the composition diagram for MnZn ferrites in mole% for Ferric oxide, Manganese oxide and Zinc oxide. It identifies the composition which gives optimum performance for saturation flux density (B_s), low losses (Q) and high initial permeability (μ_i). It also identifies the Curie temperature (T_C) lines for 100 and 250°C. From this composition chart, it is clear that not one composition, of Mn ferrite, can fulfill all design objectives.

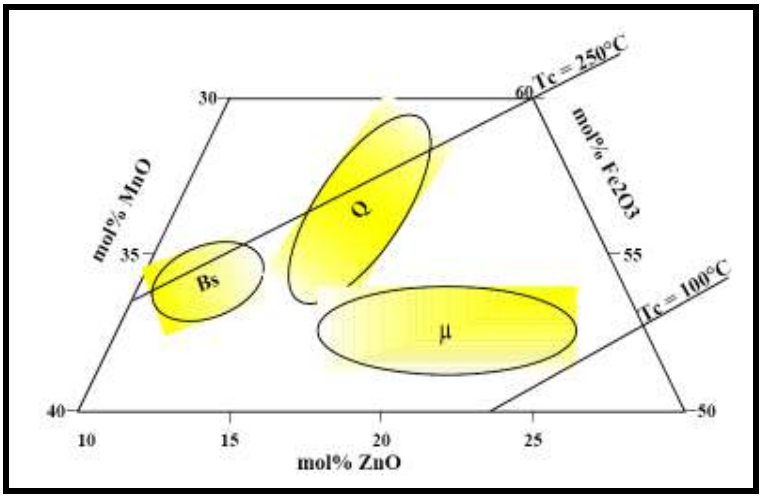

Figure 1.1 Composition Diagram for Mn-Zn ferrites.

Nickel Zinc ferrites are characterized by their high material resistivity, several orders of magnitude higher than MnZn ferrites. Because of its high resistivity NiZn ferrite is the material

of choice for operating from l-2 MHz to several hundred MHz. To cover such a wide frequency range and different applications, a large number of nickel-zinc materials have been developed over the years. Use of Nickel Zinc ferrites is limited due to their increasing cost. It should be noted that certain nickel chemistries are stress sensitive and can be adversely changed by some types of stress; this may be a mechanical shock or any grinding operations. Strong magnetic fields from holding devices and fixtures or magnetic chucks used in machining operations may also provide this stress. These resulting changes can include variation in permeability and core loss (lowering of Q). These changes cannot be reversed by degaussing or other electric/magnetic processes.

Manganese Zinc ferrite has the highest permeability and saturation induction of the ferrite class of materials and has the advantage of various stoichiometries with nearly zero magneto-crystalline anisotropy and magneto-restriction, important for stress insensitivity and low noise.

1.2 Crystal Structures of Ferrites:[1]

The crystal structure of ferrites can be regarded as an interlocking networking of positively charged metal ions (Fe^{3+} , M^{2+}) and negatively charged divalent oxygen ions (O^{2-}).The arrangement of the ions or the crystal structure of the ferrite plays an important role in determining the magnetic interactions.

1.3 Classes of Crystal Structures in Ferrites:

In ferrites, the crystal structure preferred is determined on the basis of size and charge of the metal ions that balance the charge of oxygen ions and the relative amounts of these ions. There are three crystal structures mostly available in case of ferrites. These are:

- Spinal Structure
- Garnet structure
- Hexa-ferrite structure.

1.3.1 Spinal structure:

The spinal is by far the most widely used ferrites. The spinal structure is derived from the mineral spinal ($MgAl_2O_4$ or $MgO.Al_2O_3$) whose structure was elucidated by Bragg. Analogous

to the mineral spinal the magnetic spinal have general formula $MO.Fe_2O_3$, where M is divalent metal ion. The trivalent aluminum is usually replaced by Fe^{+++} or Fe^{+++} in combination with any other trivalent ion . Although the great majority of ferrites contain iron oxide as name implies, but there are some "ferrites" based on Cr, Mn , and other elements. Although Mn, Cr are not ferromagnetic elements, in combination with other elements such as oxygen and other metal ions, they can behave as magnetic ions.

1.3.1.1 Normal Spinals:

In a unit cell of spinal lattice, eight tetrahedral and sixteen octahedral sites are occupied by metal ions. In case of mineral spinals the divalent ion (Mg) occupy the **A** site and trivalent ion (Al) occupy the **B** sites , this is known as normal spinal.

1.3.1.2 Inverse Spinals:

Barth and Posnak (1915) found many cases in which the trivalent ions preferred the **A** sites and filled these first . Spinals showing this type of structure are known as inverse spinals.

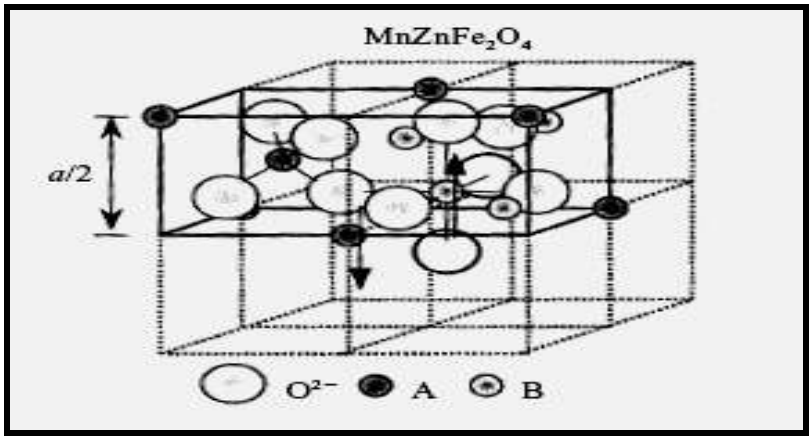

Figure 1.2 Structure of Mn-Zn Ferrite

1.3.2. Hexagonal Ferrites:

This class of magnetic oxide is called megnetoplumbite structure from the mineral of the same name. Whereas the symmetry of the spinal crystal structure is cubic, that for the megnetoplumbite structure is hexagonal. Thus, it has a major preferred axis called **C** axis. The preferred direction is used to good advantage for permanent magnetic material.

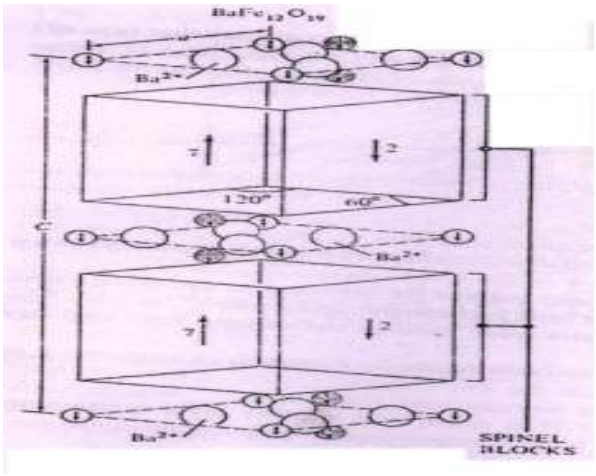

Figure 1.3 Crystal Structure of Hexagonal Mn-Zn Ferrite

The megnetoplumbite unit cell contains a total of ten layers, two of which contain M^{++} ion: four layers of oxygen ions each: followed by a layer of three oxygen ions and one M^{++} ion; again followed by four oxygen layers of four ions each: and another layer containing the three oxygen ions and one M^{++} ion but situated diametrically opposite to the M^{++} ion in the previous layer containing M^{++}.

The Fe^{+++} ions are located in the interstices of these ten layers. There are octahedral and tetrahedral sites, as well as one more type not found in the spinal structure in which the metal ion is surrounded by five oxygen ions forming a trigonal bi pyramidal in the same layer of the M^{++} ion.

The megnetoplumbite formula is $MFe_{12}O_{19}$, where M can be Ba, Sr, or Pb. There are two formula units per unit cell. Per formula unit, the moments of the 12 Fe^{+++} ions are arranged with the spins of 12 in the up direction and 8 in the down direction, giving a predicted net moment of 4 Fe^{+++} ions per formula unit time 5 per ion, or a total of 20 per formula unit.

1.3.3. Magnetic rare earth garnets:

Magnetic garnets crystallize in the dodecahedral or 12-sided structure related to the mineral garnet. The general formula is $3M_2O_35Fe_2O_3$ or $M_3Fe_5O_{12}$. Note that in this case all the metal ions are trivalent in contrast to the other two classes.In the important magnetic garnet, M is usually yttrium (Y) or one of the rare earth ions. Even though yttrium is not a rare earth ion, it behaves as one and therefore is included in the designation rare earth garnets. The ions La^{+++},

Ca^{+++}, Pr^{+++}, and Nd^{+++} are too large to form simple garnets but may form solid solutions with other rare earth garnets.

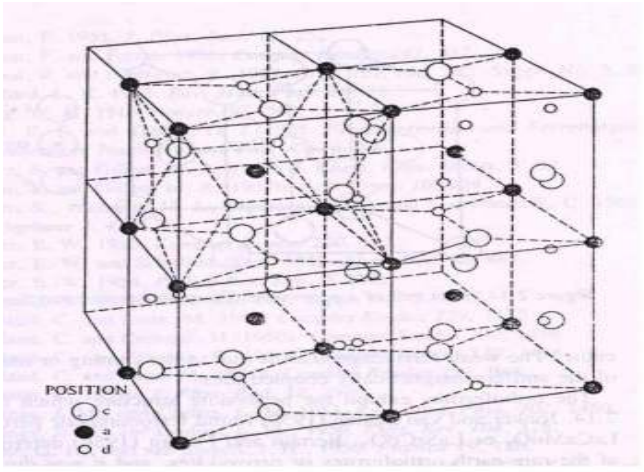

Figure 1.4 Crystal Structure of Magnetic rare earth garnet

There are three different types of sites for garnets (a) tetrahedral (b) octahedral; and (c) dodecahedral sites. The unsubstituted garnets that have only trivalent ions are very stoichiometric, so that they involve fewer preparation problems compared to the spinels.

The rare earth ions are large, and so they occupy the large dodecahedral sites. There are 16 octahedral, 24 tetrahedral, and 24 dodecahedral sites in a unit cell containing eight formula units. One formula unit, $3M_2O_3 5Fe_2O_3$, is distributed as follows:

$3M_2O_3$ –dodecahedral (c)

$3Fe_2O_3$ –tetrahedral (a)

$2Fe_2O_3$-octahedral (d)

1.4 The Magnetization in Domains and Bulk Materials

1.4.1 The nature of domains:

In a ferromagnetic domain, there is parallel alignment of the atomic moments. In a ferrite domain, the net moments of the antiferrimagnetic interactions are spontaneously oriented parallel to each other (even without an applied magnetic field). Each domain becomes a magnet composed of smaller magnets (ferromagnetic moments). Domains contain about 10^{12} to 10^{15}

atoms and their dimensions are on the order of microns ($l0^{-4}$ cm.). Domains are formed basically to reduce the magnetostatic energy which is the magnetic potential energy contained in the field lines (or flux lines as they are commonly called. Figure 1.5 shows the lines of flux in a particle with a single domain.

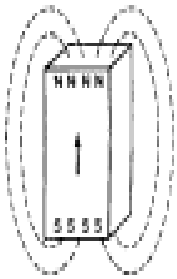

Figure 1.5 Lines of force in a particle of a single domain

The arrows indicate the direction of the magnetization and consequently the direction of spin alignment in the domain. We can substantially reduce the length of the flux path through the unfavorable air space by spitting that domain into two or more smaller domains (Figure 1.6). In Figure 1.6, the moments in adjacent domains called closure domains. When a large domain is split into *n* domains, the energy of the new structure is about *l/n th* of the single domain structure.

The size and shape of a domain may be determined by the minimization of several types of energies.They are;

- Magnetostatic energy
- Magnetocrystalline anisotropy energy
- Magnetostrictive energy
- Domain wall energy

In addition, certain microstructural imperfections such as voids, non-magnetic in-clusions and grain boundaries may also affect the local variations in domain struc-ture.

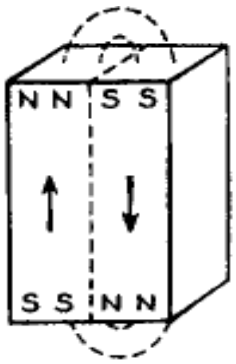

Figure 1.6 Reduction of magnetostatic energy by the formation of domains

1.4.2 Magnetostatic Energy

The magnetostatic energy is the work needed to put magnetic poles in special geometric configurations. It is also the energy of demagnetization. It can be calculated for simple geometric shapes. For an infinite sheet magnetized at right angles to the surface the equation (Bozorth 1951) for the magnetostatic energy per cm^3 is ;

$$E_p = 2\pi M_s^2$$

Neel (1944) and Kittel (1946) have calculated the magnetostatic energy of flat strips of thickness, d, magnetized to intensity, M, alternately across the thickness of the planes. The equation is;

$$E_p = 0.85\, dM^2$$

The calculations for other shapes come out with the general formula;

$$E_p = (\text{Constant}) \times dM_s^2$$

Therefore the magnetostatic energy is decreased as the width of the domain de-creases.This mathematically confirms our assumption that the splitting of domains into smaller widths decreases the energy from the magnetostatic view

1.4.3 Magnetocrystalline Anisotropy Energy:

Most matter is crystalline in nature; that is, it is composed of repeating units of definite symmetry. In most magnetic materials, to varying degree, the domain magnetization tends to

align itself along one of the main crystal directions. This direction is called the easy direction of magnetization. The difference in energy of a state where the magnetization is aligned along an easy direction and one where it is aligned along a hard direction is called the magnetocrystalline anisotropy energy.

Magnetocrystalline anisotropy is due to the fact that there is not complete quenching of the orbital angular momentum as we postulated originally. With a small orbital moment that is mechanically tied to the lattice, the spin system can couple to it and therefore indirectly affect the lattice or the dimensions of the material.

1.4.4 Magnetostrictive Energy:

When a magnetic material is magnetized, a small change in the dimensions occurs.The relative change is on the order of several parts per million and is called magnetostriction.

The converse is also true. That is, when a magnetic material is stressed, the direction of magnetization will be aligned parallel to the direction of stress in some materials and at right angles to it in others. The energy of magnetostriction depends on the amount of stress and on a constant characteristic of the material called the magnetostriction constant.

$$\mathbf{E = 3/2\ \lambda\sigma}$$

where; $\boldsymbol{\lambda}$ = magnetostriction constant and $\boldsymbol{\sigma}$ = Applied stress

1.4.5 Domain Wall Energy:

Bloch in 1932 present the idea of magnetic domains, with domain walls (sometimes called Bloch walls) or boundaries separating them. In the domain structure of bulk materials, the domain wall or boundary is that region where the magnetization direction in one domain is gradually changed to the direction of the neighboring domain. If 5 is the thickness of the domain wall which is proportional to the number of atomic layers through which the magnetization is to change from the initial direction to the final direction, the exchange energy stored in the transition layer due to the spin interaction is;

$$\mathbf{E_e = kT_c/a}$$

Where $\mathbf{kT_c}$ = thermal energy at the Curie point and **a** = Distance between atoms

Therefore the exchange energy is reduced by an increase in the width of the wall or with the number of atomic layers in that wall. However, in the presence of an anisotropy energy or preferred direction, rotation of the magnetization from an easy direction increases the energy so the wall energy due to the anisotropy is:

$$\mathbf{E_k = k\,\delta}$$

In this case, the energy is increased as the domain width or number of atomic layers is increased. The two effects oppose each other and the minimum energy of the wall per unit area of wall occurs according to the following equation;

$$\mathbf{E_w = 2\,(K_a T_c/a)^{1/2}}$$

Where, $\mathbf{K_a}$ = Anisotropy constant

If magnetostriction is a consideration, the equation is modified to;

$$\mathbf{Ew = 2\,(kT/a)^{1/2}\,(K_a + 3\,\lambda_s \sigma/2)^{1/2}}$$

where λ_s= magnetostriction constant

Typical values of domain wall energies are on the order of **1-2 ergs/cm^2**. The domain wall thickness for the condition of minimum energy is given by the equation;

$$\mathbf{\delta = (constant)\ x\ a\,(E/K)^{1/2}}$$

Typical calculated values of **δ** are about 10^3 A^0 or about 10^{-5} cm. With some soft magnetic materials the value may be about 10^{-6} cm while in some hard materials, the value may be on the order of $l0^{-4}$ cm. or about one micron. The whole array of domains will be arranged in such a way as to minimize the total energy of the system composed mainly of the above four energies.

1.5 Hysteresis behavior:

In magnetic materials if we start with a demagnetized specimen and increase the magnetic field, the induction increases as shown in Figure 1.7. At high fields, the induction flattens out at a value called the saturation induction, Bs. If, after the material is saturated, the field is reduced to zero and then reversed in the opposite direction, the original magnetization curve is not

reproduced but a loop commonly called a hysteresis loop is obtained. Figure 1.7 shows such a hysteresis loop with the Initial magnetization curve and hysteresis loop magnetization curve included. The arrows show the direction of travel. We notice that there is a lag in the induction with respect to the field. This lag is called hysteresis. The area included in the hysteresis loop is a measure of the magnetic losses incurred in the cyclic magnetization process.

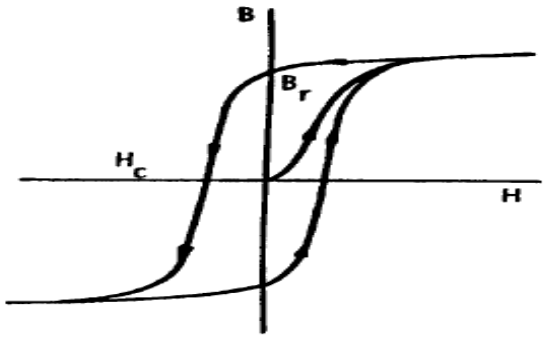

Figure 1.7 Initial magnetization curve and hysteresis loop

The value of the induction after saturation when the field is reduced to zero is called the remanent induction or remanence or retentivity, (B_r). The values of the reverse field needed after saturation to reduce the induction to zero is called the coercive force or coercivity, (H_c). Both of these properties are very important and we shall refer to them in almost every magnetic application.

CHAPTER-2

LITERATURE SURVEY

2.1 Recent Work On the Synthesis of Mn-Zn Ferrites:

Nano Mn-Zn ferrite has been prepared and magnetic properties have been listed by the several authors.

Chen and Chang[2], reported that the zinc loss will reduce the initial permeability from 11,000 to 6,000. The key sintering parameters increasing this zinc loss are low oxygen atmosphere in high

temperature, high gas flow rate in the furnace and the reaction of zinc oxide with Algol. Minimizing zinc loss during sintering is of paramount importance to the successful preparation of high permeability Mn-Zn ferrites.

Skolyszewska et al. synthesized[3] a $(Mn_{0.55}Zn_{0.3}5Fe_{0.1})Fe_2O_4$ ferrite by the powder mixing method and calcinations at 900–1050 °C for 1.5 h, followed by grinding, mixing the powder with organic dispersants (sodium acrylate) and binders, granulation by spray-drying, lubrication of granules with zinc stearate, pressing into toroidal specimens (8 MPa) and sintering in air at 1250–1300 °C for 4.5–5.5 h and cooling down in air as well. They obtained dual phase ferrite: jacobsite [$MnFe_2O_4$] and iwakiite [$MnFe_2O_4$] were identified together with Fe_2O_3 particles inside de manganese–zinc ferrite matrix, whose grain sizes were in the range of 3 to 9 μm.

R. Arulmurugan[4] prepared $Mn_{(1-x)}Zn_xFe_2O_4$ (x=0.1-0.5) nanoparticles less than 12nm are by chemical co-precipitation method which could be used for ferrofluid preparation. He found that the particle size decreases with the increase in the Zn concentration for Mn–Zn ferrites. The estimation of associated water content, which increases with the Zn concentration, plays a vital role for the correct determination of cation contents. The Curie temperature and the temperature at which maximum value of thermomagnetic coefficient was observed decreased simultaneously with the increase in the initial substitution of zinc.

A. K. Singh et. al [5] synthesized polycrystalline $Mn_xNi_{0.5-x}Zn_{0.5}Fe_2O_4$ (x = 0.05 to 0.45) by the non-conventional citrate precursor method. The staring materials were manganese nitrate (98.5%, Merck, Germany), zinc nitrate (96%, Merck, India), nickel nitrate (97%, Merck, India), iron (III) citrate (Merck, Germany) and citric acid (99.5%, Merck, India).

X-ray diffraction of all samples were taken which confirmed the single-phase structure of ferrites. The grain sizes obtained in their work for the samples sintered at 1200°C are in the range 0.5–2 μm, which are much smaller than those for the samples prepared by the conventional ceramic method. The ferrite particles prepared by citrate precursor method being small in size, a tendency towards agglomeration is observed. Smaller grains result in large number of grain boundaries, which act as scattering centers for the flow of electrons and therefore decrease the conductivity.

The value of dielectric constant was found around 15 which is more than 10^3 times lower than those usually reported for ferrites obtained by the conventional ceramic method. This low value of dielectric constant is attributed to the method of preparation, i.e., the citrate precursor method.

Ming Ma, et. al [6] prepared Mn-Zn ferrite nanoparticles with stearic acid gel method. The obtained samples were characterized by energy dispersive X-ray spectroscopy (SEM-EDS), X-ray diffraction (XRD) and transmission electron microscopy (TEM). Results show that spinel structure of Mn-Zn ferrite has formed.

Mn-Zn ferrite ($Mn_xZn_{1-x}Fe_2O_4$) nanoparticles were prepared by following procedure. Measured amounts of $MnCO_3$, $Zn(NO_3)_2$.$6H_2O$ and $Fe(NO_3)_2$.$9H_2O$ (molar ratio of Mn:Zn:Fe=3:2:10) were grinded into powders and then added to molten stearic acid. The mixture was heated in oil bath at 120°C and stirred for 3-4 hours. After that a brown gel was obtained. The gel was cooled in air and grinded into powder. This powder was then washed with ethanol three times and dried at 100°C. Finally, black magnetic Mn-Zn ferrite was obtained by heating at 450°C for 1 hour. The ratio of Mn, Zn and Fe in the Mn-Zn ferrite obtained was determined to be 0.62:0.38:2 by SEM-EDS elemental analysis as expected by the preparation method. Consequently, the Mn-Zn ferrite obtained can be expressed as $Mn_{0.62}Zn_{0.38}Fe_2O_4$.

The calculated ACD value was 6 nm in agreement with TEM results the diameter of the Mn-Zn ferrite nanoparticles in the range of 4-9 nm The magnetic properties of the Mn-Zn ferrite nanoparticle powder were measured by VSM. From VSM experiments, the magnetic parameters such as saturation magnetization (Ms), coercivity (Hc) and remnant magnetization (Mr) were obtained which are given in Table 2.1 below.

Table 2.1 Magnetic properties of the samples

Sample	Ms(emu g^{-1})	He (Oe)	Mr(emu g^{-1})
Mn-Zn	21.3	109.6	1.79

The particles obtained by this process are rather large and non-uniform in size. The size of obtained particles is about 6 nm in diameter with a narrow size distribution.

Dong Limin et. al [7] synthesized Mn-Zn spinel ferrites by sol-gel method and also investigated the effect of calcination temperature on structure and particle size of $MnZnFe_2O_4$. These particles

were analyzed by X-ray diffraction (XRD) and scanning electron microscopy (SEM) . The particle size becomes larger with the increase of calcination temperature and the distribution of particles becomes even more homogeneous. Sintering behavior of synthesized ferrite powders depend on the powder characteristics and high temperatures have induced the good crystallization of particles.

Figure 2.1 shows the SEM images of Mn-Zn ferrite prepared by the sol-gel process with different calcined temperature. In fact, these images not only exhibit the shape and size of the samples, but also give the intermediate shape change during the formation process of the compounds. It can be seen that the gain size becomes larger with the increasing the calcination temperature, as shown in Figure 2.1(a - d) . It indicates that particles are fairly uniform and the size of the Mn-Zn ferrite powder fired at 900°C is in the range of 60 - 90 nm as shown in Figure 2.1(a)

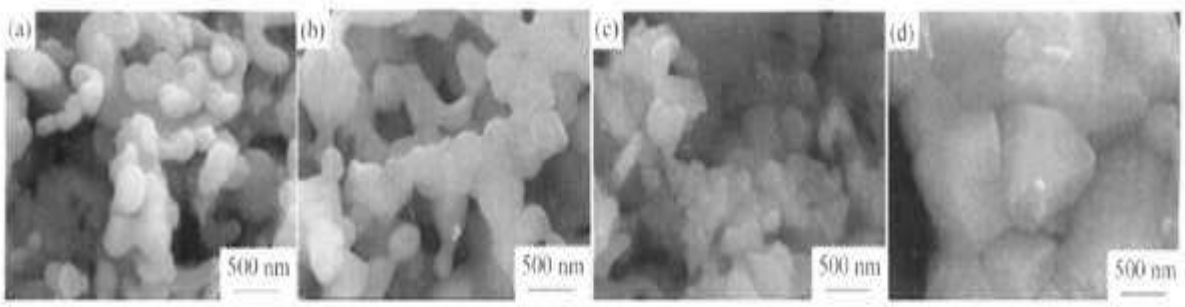

Figure 2.1 SEM micrograph of powder calcined at **(a)** 900°C **(b)** 1000°C **(c)** 1100°C **(d)** 1200°C

Their method provides simple, fast, and low temperature synthesis and thus formed nano-size particles of powders. Single phase spinel cubic Mn-Zn ferrite is formed by direct crystallization from amorphous materials and no deterimental intermediate phase is observed. Different particle size of Mn-Zn ferrite powders has been synthesized by varying the calcinations temperature and the gain size becomes larger with the increasing of calcined temperature.

M. Mozaffari, et. al [8] prepared $Mn_{1-x}Zn_xFe_2O_4$ ($0 < x < 1$) nanocrystalline powders via mechanochemical processing. The raw materials, Fe_2O_3 from a domestic source, MnO_2 and ZnO, both from the Merck Company, were milled in a high-energy mill in air and annealed in various atmospheres and temperatures in order to achieve single-phase samples. Mean crystallite sizes of the annealed powders were calculated from XRD patterns, using Scherrer's formula. Magnetic

measurements were performed on cold pressed samples and saturation magnetization was obtained. Also using an LCR-meter, the Curie temperature of each sample was measured.

In their work they have taken MnO_2 and ZnO from the Merck Company and Fe_2O_3 from a domestic source as the starting materials. A total of 4 g of the raw materials together with four 9mm and three 12mm hardened steel balls was loaded in a hardened steel vial in air and milled for 5 h in a SPEX 8000D mixer/mill. The milled powders, with different *x*, were annealed at different temperatures to obtain a single-phase powder. The nanocrystalline powder was in the range 25–35 nm in size.

In order to obtain a single-phase ferrite, the as-milled powders were annealed at different temperatures. For annealing temperatures higher than 700°C, the peak intensities corresponding to spinel phase start to increase and those corresponding to other phases decrease. Ultimately by increasing the annealing temperature to 1025°C a single-phase ferrite is achieved.

They also investigated the variation of minimum annealing temperature with respect to *x* (Zn content) to achieve a single-phase ferrite and found a smooth increase in particle size with respect to *x* has occurred. This is due to the fact that as the value of *x* increases, the minimum annealing temperature increases.

The variation of saturation magnetization (*M*s) with *x* at room temperature has also been taken in their study. They found the variation is exactly the same as the variation of *M*s of the powders prepared by co-precipitation .

They also studied the variations of Curie temperature (T_C) for the prepared samples with respect to Zn content and the results show that with increasing *x*, *T*c starts to decrease. This is because of the replacement of more non-magnetic ions (Zn^{2+}) instead of Mn^{2+} in the A site.

The main consequences of their work is that, Ms variations of the nano-sized Mn-Zn ferrite powders prepared by MCP are exactly the same as the variations of *M*s correspond to nanopowders prepared by coprecipitation. The second important result is the variation of T_C with *x*, which again is similar to the T_C of the powders prepared by coprecipitation method.

I.P.Kilbride and R. Freer [9] prepared Manganese–zinc ferrite ($Mn_{0.52}Zn_{0.4}1Fe_{2.07}O_4$) by the mixed-oxide route. Specimens were in the form of toroids, pressed in the green state to 11.9 mm

outside diameter and 5.9 mm inside diameter. To assess the effect of zinc loss, they employed, a variety of circular local sintering enclosures. All specimens were initially sintered in air at 1390°C for times of 7.5–16 hours. After cooling to 1200 C they were held for 4 hours in atmospheres containing 0.0125–0.05% oxygen. Sintered products were single-phase, with density greater than or equal to 95% theoretical and a grain size of about 20μm.

Setsuo Yamamoto et al. [10] successfully fabricated Mn–Zn ferrite platelet cores with few vacancies using spark-plasma-sintering (SPS) method. Laminated cores composed of Mn–Zn ferrite were prepared which show large saturation magnetic flux density and high permeability at high frequencies. These soft magnetic cores maybe available as the magnetic cores of a magnetic head used in a card reader or the soft magnetic substrates of the perpendicular recording hard disks.

S.H. Keluskara et al. [11] reported that nano-particle ferrite having general formulae $Mn_xZn_{1-x}Fe_2O_4$ with x = 0.35 / 0.40 / 0.45 / 0.55 / 0.60/ 0.65 were prepared using nitrilo-triacetate precursor method. Production of fine grain size material at low temperature is the unique feature of this method. Bulk $Mn_xZn_{1-x}Fe_2O_4$ ferrite material produced by sintering nanoparticles at 950 / 1050 / 1150 / 1250 / 1350 ^{O}C progressively in nitrogen atmosphere showed high values for initial permeability.

The microstructural development and magnetic properties of MnZn ferrites doped with various amounts of CaO and sintered in atmospheres containing various oxygen concentrations were also investigated.Their results indicate a strong link among the amount of CaO segregated in the grain boundary, the oxygen concentration during sintering, the average grain size, and the magnetic properties of the MnZn ferrites.

Nobuyuki Kikukawa, et al.[12] prepared zinc-substituted spinel-type ferrite fine particles of $M_{1-x}Zn_xFe_2O_4$ (M=Mg, Mn, Co, Ni, Cu) with good crystallinity and stoichiometry, by a glycine–nitrate process. The product powder was an agglomerate of fine particles whose typical diameter was several tens of nanometers. X-ray diffraction patterns revealed that the produced particles were mono-size in almost all reaction systems. Energy-dispersive X-ray spectroscopy microanalysis of the product particles (Mn–Zn–Fe–O) revealed that the distributions of Mn/Fe ratio and Zn/Fe ratio were highly sharp both within the agglomerate and between agglomerates.

R. Justin Joseyphus[13] synthesized size-controlled $Mn_{0.67}Zn_{0.33}Fe_2O_4$ nanoparticles in the wide range from 20 to 80 nm, for the first time, using the oxidation method. They demonstrated that the particle size can be tailor-made by varying the concentration of the oxidant. The magnetization of the 80 nm particles was 49 A m^2 kg^{-1} compared to 34 A m^2 kg^{-1} for the 20 nm particles. The Curie temperatures for all the samples were found to be within 630±5 K suggesting that there is no size-dependent cation distribution. The critical particle size for the superparamagnetic limit is found to be about 25 nm. The effective magnetic anisotropy constant is experimentally determined to be 7.78 kJ m^{-3} for the 25 nm particles, which is about an order of magnitude higher than that of the bulk ferrite.

Wang Xin,[14] investigated the density, microstructure and magnetic properties of non-doped Mn-Zn ferrite nanoparticles sintered compacts. The compacts of non-doped Mn-Zn ferrite nanoparticles were sintered by segmented-sintering process at lower sintering temperature. They measured the density of sintered samples by Archimedes method, the phase composition and microstructure were examined by XRD and SEM. The sintered Mn-Zn ferrite magnetic measurements were carried out with vibrating sample magneometer. The results show that the density of sintered compacts increases with the rising of sintering temperature, achieving 4.8245 $g.cm^{-3}$ when sintered at 900 T , which is the optimal density of Mn-Zn functional ferrite needed and from the fractured surface of sintered samples, it can be seen that the grain grows well with small grain size and with homogeneous distribution. The sintering temperature (900°C) is 450°C lower than that of conventional sintering process(1350°C). In this way, it can save much energy resources.

The crystal structure of the samples sintered at different temperature were examined by X-ray diffraction indicating that all samples have single phase spinel structure and no unreacted constituents were present in these samples.

They also studied the microstructure of Mn-Zn ferrite sintered samples and from the fractured surface of sintered samples sintered at 900°C they concluded that grain grows well with homogeneously distributed phases.(Figure 2.2).

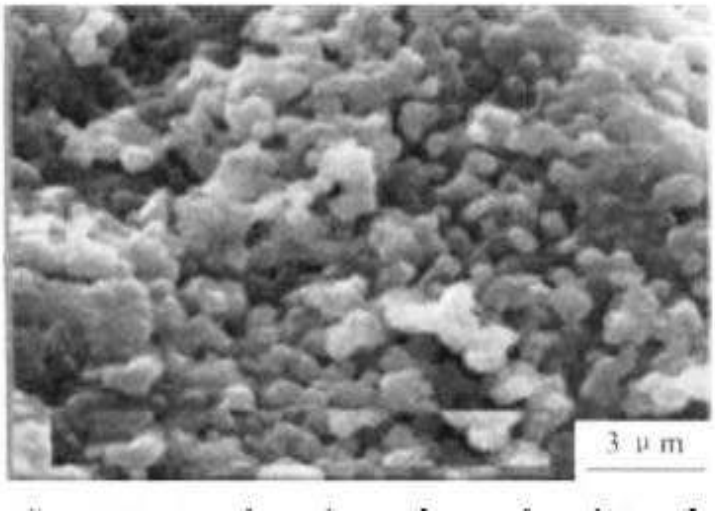

Figure 2.2 SEM of the fractured surface of Mn-Zn ferrite sample

Goldman et al.[15] invented a process for ferromagnetic materials and pressure compacted soft ferrite components utilizing a "wet process" for compositional preparation of materials in which metal carbonates and metal hydroxides are co-precipitated in controllably selected ratios.

Their invention provides a wet process for preparing an intermediate product convertible to ferromagnetic material for use, and specially suitable for manufacture of soft ferrite components by pressure compaction.

In their wet process an aqueous solution of ferrous ions and other divalent metal ions is formed. This metal ion solution reacted to coprecipitate ferrous and other divalent metal carbonates while concurrently coprecipitating ferrous and other divalent metal hydroxides. This simultaneous coprecipitation of metal carbonates is accomplished essentially without coversion of ferrous ions to ferric ions.

B. Parvatheeswara Rao, et. al [16] prepared two mixed ferrite systems, namely $Ni_{0.65}Zn_{0.35}Fe_2O_4$ (Ni–Zn) and $Mn_{0.75}\ Zn_{0.18}\ Fe_{2.07}\ O_4$ (Mn–Zn) by coprecipitation method, and then the resulting ultrafine powders were heat treated at different temperatures from 200 to 800°C for improved crystallinity and magnetic properties.

As a result of the heat treatment, the average particle size has been found to increase from 9.9 to 15.7 nm for Ni–Zn ferrites and from 2.4 to 10.2 nm for Mn–Zn ferrites, and the corresponding

magnetization values have increased from 9.1 to 23 emu/g for Ni–Zn ferrites and from 7.9 to 11.7 emu/g for Mn–Zn ferrites, respectively. The results are discussed in the light of changes in particle size and inversion degree parameter for cationic distribution at nanoscales.

Kinnari Parekh, et. al [17] for the first time synthesized a ternary system of $Mn_{0.5}Zn_{0.5}Fe_2O_4$ using thermal decomposition of metal acetylacetonate in the presence of a high temperature boiling point solvent and fatty acids (Figure 2.3).

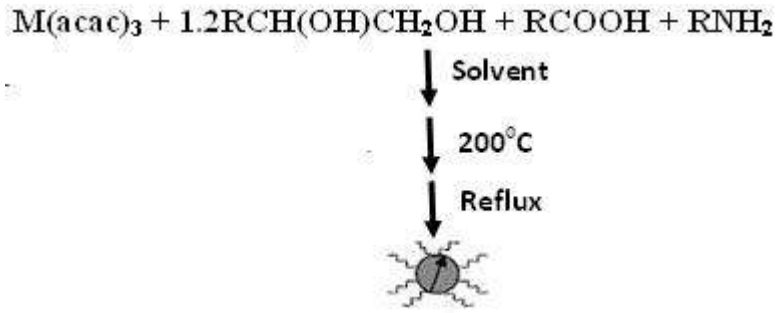

Figure 2.3 Schematic diagram of synthesis of magnetic particles

Unlike the results of synthesis of this material by other techniques, they obtained nearly monodispersed nanoparticles, rendering them ideal for applications like in hyperthermia. The crystal structure and morphology of the particles were determined using x-ray diffraction (XRD) and transmission electron microscopy (TEM). The XRD results confirm a single phase spinel structure with no other impurity phases as shown in Figure 2.4. The particles are of 7 nm average diameter, with a very narrow (<10%) size distribution. The oleic acid surfactant on the particles shows a 28% weight loss in thermo gravimetric analyses (TGAs), which corresponds to a monolayer thickness of the coating. Magnetic measurement shows that the particles are super paramagnetic with a characteristic blocking temperature of around 50 K.

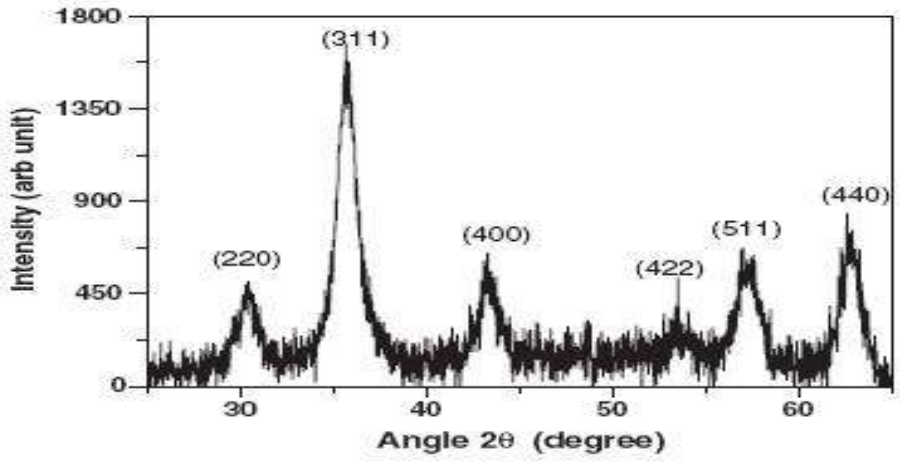

Figure 2.4 XRD pattern for synthesized $Mn_{0.5}Zn_{0.5}Fe_2O_4$

S. Otobe, et. al [18] studied relations between the microstructure and core loss of Mn-Zn ferrites for power supplies. They found that the lowest core loss was achieved at 100 kHz and 200 mT condition when the average grain sizes were 15 to 11 μm. They examined the effect of the third element in addition to $CaO\text{-}SiO_2$ on their deposition behavior. At the grain boundary they found some additives such as Nb_2O_5, Ta_2O_5 and ZrO_2 which reduce the core losses. Further more, by optimizing the sintering condition they were able to obtain the extremely low loss Mn-Zn ferrite material for power applications.

2.2 Summary of the literature survey:

The results of the literature survey can be summarized in the following manner;

(1). The particle size become larger with the increasing the calcination temperature and the distribution of the particles become even more homogeneous.

(2). Different particle size of Mn-Zn ferrite powders has been synthesized by varying the calcinations temperature and the grain size become larger with the increasing the calcined temperature.

(3). Sintering behavior of the ferrite powder depends on the powder characteristics and high temperatures have good crystallization of particles. Also the density of the sintered compact increases with the rising of sintering temperature.

(4). Higher sintering temperature results in the bigger grains and in conventional ceramic method, the sintering temperature being higher results in bigger grains.

(5). The particle size decreases with increasing the Zn concentration for Mn-Zn ferrites. This was probably due to the reaction conditions which favored the formation of the new nuclei preventing the further growth of the particles when Zn concentration was increased.

(6). The curie temperature at which the maximum value of thermomagnetic coefficient was observed decreases simultaneously with the increase in the initial substitution degree of Zinc. This is because of the replacement of more non-magnetic ions (Zn^{2+}) instead of Mn^{2+} in the A site.

(7). The magnetization of ferrite nanoparticles synthesized by co-precipitaion method depends mostly on the parameters such as reaction temperature, pH of the suspension, initial molar concentration etc.

(8). The concentration of Mn^{2+} and Fe^{3+} deviates from their stoichimetry when higher pH is used for precipitation.

(9). Preparation conditions serves as an effective means to have a control over the particle size or in other words the precipitation technique of nanoparticles has a definite impact on the control of the particle size and alternation of magnetic properties.

(10). Smaller grains results in larger number of grain boundaries, which act as scaterring centres for the flow of the electrons and therefore decreases the conductivity.

(11). For the reduction of hysteresis losses the sintered products should have relatively large and uniform grains without the lattice defects or pores so as not to hinder the movements of the domain walls. Also the sintered density is as high as possible.

(12). The eddy current losses is proportional to the cross section area of the grains, i.e. square of the grain size.

(13). In addition to the well-known additives of CaO and SiO_2, a small amounts of additives such as Nb_2O_5, Ta_2O_5, and ZrO_2, which further reduce the core losses. These additives enhance the segregation of CaO in the grain boundary region, and as the result magnetic characteristics of ferrites were improved.

The results obtained by the various synthesis methods can be summarised in the form of a table. Table 2.2 shows the synthesis results of Mn-Zn ferrite material synthesized by some methods.

Table 2.2 Synthesis results of Mn-Zn ferrite by different methods

S.No.	**Synthesis Method**	**Particle size**	**Phase identified**
1	Powder mixing[3]	3-9 μm	Jacobsite and iwakiite
2	Chemical coprecipitation[4]	< 12 nm	Cubic spinel structure
3	Non conventional citrate precursor method[5]	0.5-2 μm	Single phase Spinel
4	Steric acid gel method[6]	4-9 nm	Spinel structure
5	Sol-gel method[7]	60-90 nm	Spinel cubic structure
6	Mechanochemical method[8]	25-35 nm	Single phase spinel
7	Mixed oxide route[9]	20 μm	Single phase spinel

8	Oxidation method[13]	20-80 nm	Spine structure
9	Thermal decomposition[17]	7 nm	Single phase spinel

CHAPTER-3

EXPERIMENTAL WORK

3.1 Raw Material:

Mn-Zn ferrite was synthesized through chemical route. The synthesis was done by the chemical copercipitation method. For the synthesis of $MnZnFe_2O_4$ particles from the pure chemicals the salts of constituent metals have been taken as starting materials. The metallic salts used are iron (III) chloride hexahydrate ($FeCl_3.6H_2O$) , manganese (II) chloride tetrahydrate ($MnCl_2.4H_2O$) and zinc chloride ($ZnCl_2$). All the salts used were of analytical grade .The purity of iron chloride, manganese chloride and zinc chloride salts were 96%, 99% and 96% respectively. The base used was sodium hydoxide (NaOH) which was used as reducing agent. While for the synthesis of the Mn-Zn ferrite from the blue dust the blue dust has been taken in place of Iron (III) chloride hexahydrate ($FeCl_3.6H_2O$) and hydrochloric acid is used to convert it into Iron (III) chloride.

3.2 Apparatus used:

The appratus used for the synthesis of Mn-Zn ferrite material in the laboratory is simply a magnetic stirrer with hot plate which is shown in the Figure 3.1. With the help of this stirrer the stirring can be done simultaneously with heating at desired temperature upto 100°C.

Figure 3.1 Magnetic stirrer with hot plate

3.3 Experimental Procedure:

The synthesis has been done with two different types of the materials i.e. from the pure chemicals and from the blue dust as iron source. The procedure used for these two are given below.

3.3.1 Synthesis from Pure Chemicals:

$Mn_{0.5}Zn_{0.5}Fe_2O_4$ fine particles were prepared by the chemical coprecipitation method. Aqueoous solution of $MnCl_2$, $ZnCl_2$ and $FeCl_3$ were prepared. The molar concentration of these solutions were prepared as 0.055M, 0.055M and 0.11M respectively in separate beakers. After that $ZnCl_2$ solution was mixed into the $MnCl_2$ solution at the room temperature and the resuting solution was mixed into the $FeCl_3$ solution. Now the solution of sodium hydroxide with molarity 0.725M was made and was allowed to heat until the temperature reached to 80^0C. Then the resulting solution of $MnCl_2$, $ZnCl_2$ and $FeCl_3$ was added into the boiling solution of NaOH and temperature of the resulting solution was maintained at 80^0C followed by continuous stirring. The pH of the final solution is maintained around 12 and stirring was continued. This process is done for the stirring time 2hrs, 3hrs and 4hrs. Precipitation and formation of nanoferrites takes place by the conversion of metal salts into hydroxides, which occurs immediately followed by transformation of hydroxides into ferrites. After completion of the reaction the solution was filtered and washed many times with the distilled water. The particles were dried at 50^0C for 3-4 hrs. The flow sheet for the synthesis of the Mn-Zn ferrite by the chemical coprecipitation method from the pure chemicals is given in the Figure 3.2.

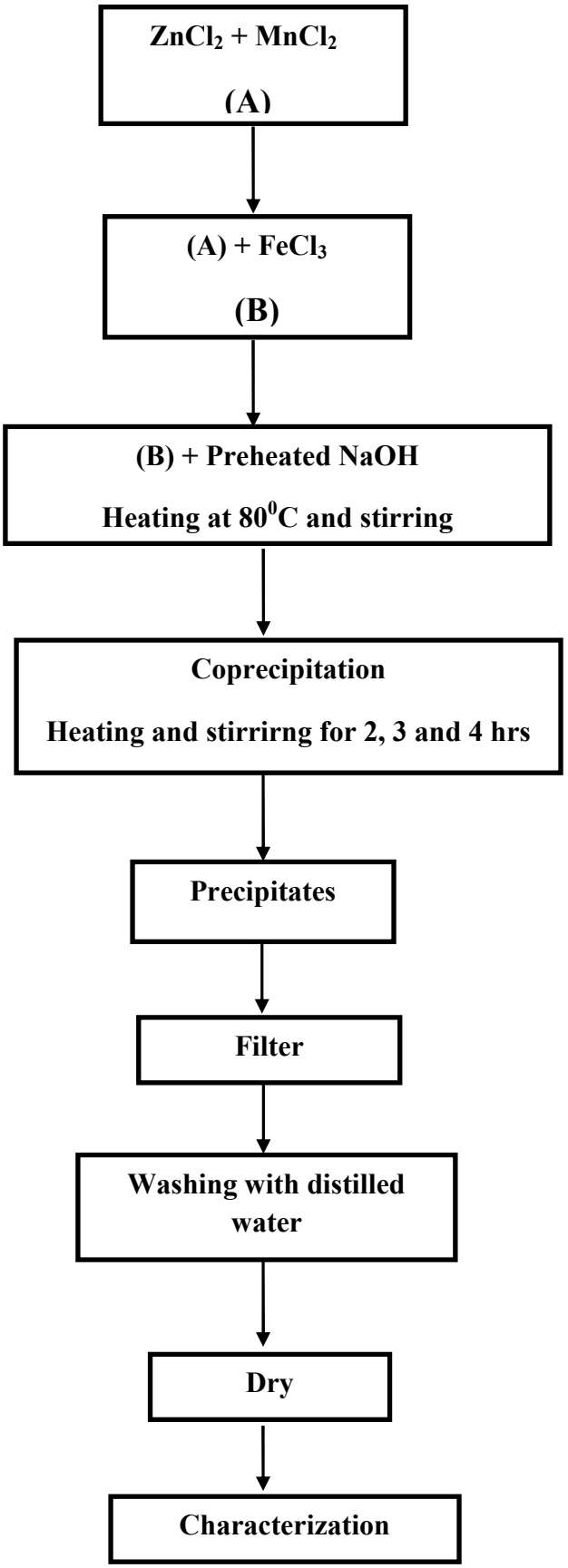

Figure 3.2 Schematic diagram for synthesis of Mn-Zn ferrite from pure chemicals

3.3.2 Synthesis from Blue Dust:

Blue dust is iron ore fines and is found abundantly in the iron ore mines. It cannot be used directly in steel making process due to the fineness of the particle. Many of the mines just dispose off in tailing dumps. However, due to its high purity and suitability for powder metallurgical process, it may be beneficially utilized for the preparation of ferrites. The blue dust contains more than 95% iron oxide. The high iron content in grade of iron ore fines with silica open up the scope of effectively utilizing it to prepare soft ferrites, which will have great economic impact.

In the blue dust iron is present in the form of iron oxide (Fe_2O_3) which can be used for the synthesis of Mn-Zn ferrite. This iron oxide has to be converted into chloride form. First of all the required amount of the blue dust was taken and it was heated with the concentrated hydrocloric acid. After the completion of the reaction blue dust was converted into the ferric chloride which was then filtered. The remaining procedure was same as that for the pure chemicals. The prepared solutions of $MnCl_2$, $ZnCl_2$ were mixed into the $FeCl_3$ solution. The resulting solution was then added into boling NaOH solution and the temperature of the solution was maintained at 80^0C followed by continuous stirring. The pH of the solution was maintained around 12 the stirring was done for 3 hrs. Then the particles were filtered and washed with distilled water and dried at 50^0C for 4 hrs. The flow sheet for the synthesis of the Mn-Zn ferrite by the chemical coprecipitation method using blue dust is given in the Figure 3.3.

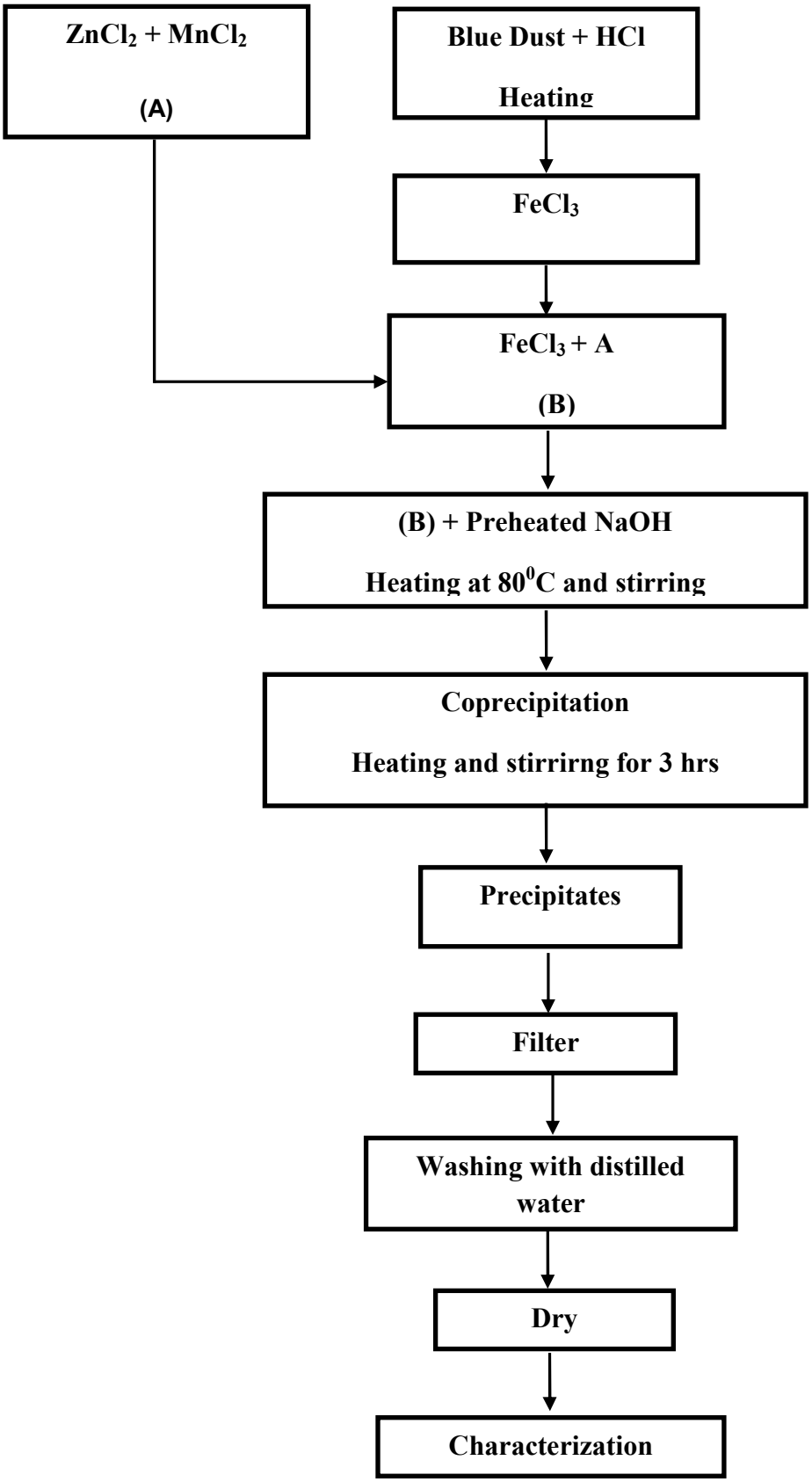

Figure 3.3 Schematic diagram for synthesis of Mn-Zn ferrite from blue dust.

3.4 Characterization Techniques:

3.4.1 X-ray diffraction analysis:

X-ray diffraction analysis (XRD) is a non-destructive, very versatile technique to determine the crystalline phases and their volume fractions. The sample is irradiated with monochromatic X-rays and the reflected radiation is recorded by the counters. In this techniques various forms of the samples could be used and very less amount is required for the phase determination. The x-ray diffraction patern were recorded using Rigaku model Geiger diffractogram with CuK_{α} radiation (λ = 1.5418 Å) obtained from the copper target using an in built Ni filter. The 2θ values for XRD paterns were generally taken in the range of 5° to 100 ° for most of the samples at a scan rate of 5 ° per min. The inter planar spacing (d) values of samples were calculated using Bragg's law.

$$2d\sin\theta = n\lambda$$

where λ is the wavelength of the incident X-ray, d is the inter planar distance and θ the diffraction angle. The XRD patterns were identified using Powder Diffraction files (PDF). The geometric representation of Bragg's law is given in the Figure 3.4.

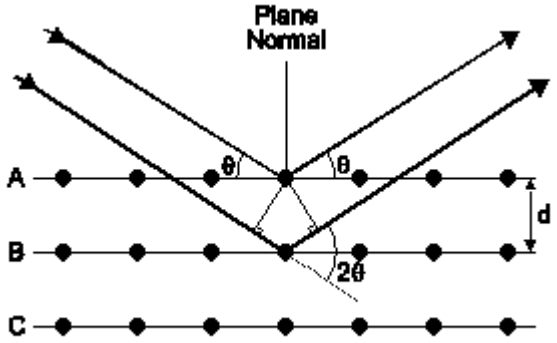

Figure 3.4 Geometric representation of X-ray diffraction

3.4.2 Scanning Electron Microscope*:*

The scanning electron microscope (SEM) is a type of electron microscope that images the sample surface by scanning it with a high-energy beam of electrons in a raster scan pattern. The electrons interact with the atoms that make up the sample producing signals that contain information about the sample's surface topography, composition and other properties such as electrical conductivity.

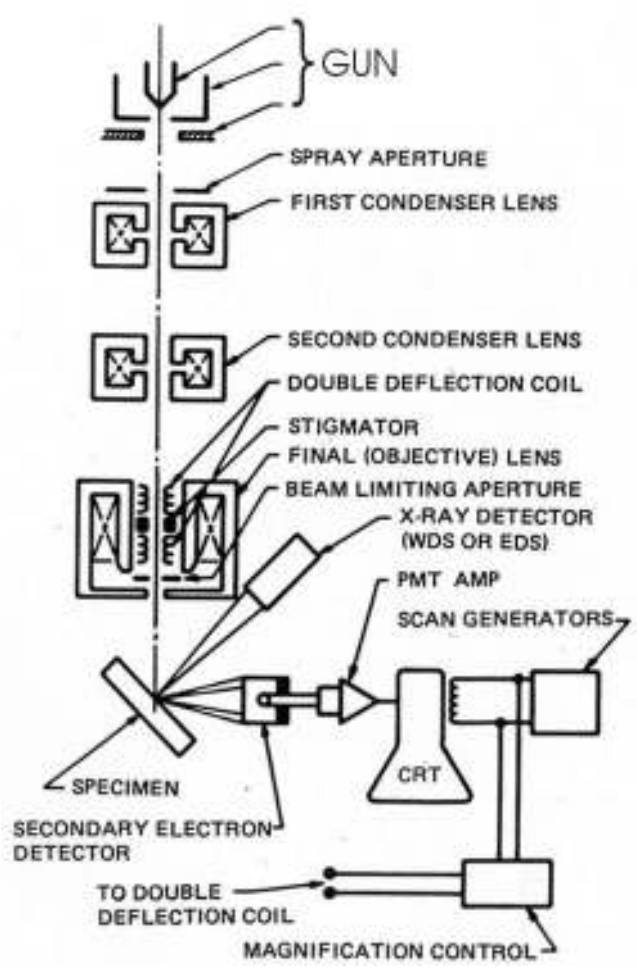

Figure 3.5 Scanning Electron Microscope

The types of signals made by an SEM can include secondary electrons, back scattered electrons, characteristic X-rays and light (cathodoluminescence). These signals come from the beam of electrons striking the surface of the specimen and interacting with the sample at or near its surface. In its primary detection mode, secondary electron imaging, the SEM can produce very

high-resolution images of a sample surface, revealing details about 1 to 5 nm in size. Due to the way these images are created, SEM micrographs have a very large depth of focus yielding a characteristic three-dimensional appearance useful for understanding the surface structure of a sample. This great depth of field and the wide range of magnifications (commonly from about 25 times to 250,000 times) are available in the most common imaging mode for specimens in the SEM.

The operation of a SEM is schematically depicted in Figure 3.5. A beam of electrons is generated by an electron gun located at the top of the beam column. This beam is accelerated to the anode, condensed with a condenser lens, and focused to a very fine spot on the sample by the objective lens. The scan coils, by varying the voltage produced by the scan generator, create a magnetic field, which deflects the beam back and forth in a controlled pattern. The varying voltage is also applied to the coils around the neck of the cathode-ray tube (CRT), which produces a pattern of light deflected back and forth on the CRT. In this way, the pattern of deflection of the electron beam is the same as the pattern of deflection of the spot of light on the CRT. SEM images can be generated by any signal produced by the interaction of a finely focused primary beam of electrons as it is scanned over the sample surface.

3.4.3 Transmission Electron Microscope:

Transmission electron microscopy (TEM) is a microscopy technique whereby a beam of electrons is transmitted through an ultra thin specimen, interacting with the specimen as it passes through it. An image is formed from the electrons transmitted through the specimen, magnified and focused by an objective lens and appears on an imaging screen.

A TEM (transmission electron microscope) uses a highly energetic electron beam (100 keV - 1 MeV) to image and obtain structural information from thin film samples. The electron microscope consists of an electron gun, or source, and an assembly of magnetic lenses for focusing the electron beam. Apertures are used to select among imaging modes and to select features of interest for electron diffraction work. The sample is illuminated with an almost parallel beam of electrons, which is scattered by the sample. In crystalline materials, the scattering takes the form of one or more Bragg diffracted beams, which are used to form a transmission diffraction pattern. These diffraction patterns can be used to identify unknown

phases in the sample. A bright-field image of the sample can be formed by looking at the straight-through, non-diffracted beam. Features in the sample that cause scattering have darker contrast in a bright-field image than those that cause little or no scattering. An electron diffraction pattern can be generated from a particular area in a bright-field image (such as a particle or grain) by using a selected area aperture. Dark-field images are formed from a single diffracted beam and are used to identify all the areas of a particular phase having the same crystalline orientation. Magnifications from about 100X up to several hundred thousand times can be achieved in the TEM. The schematic diagram of the TEM is given in Figure 3.6.

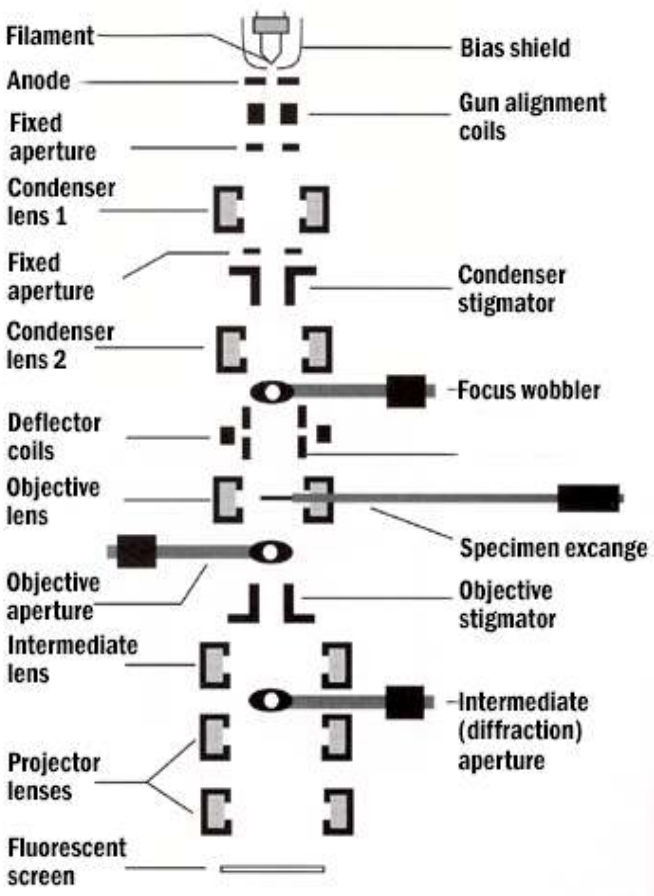

Figure 3.6 Schematic ray diagram of TEM

3.4.4 Differential Thermal Analysis:

Differential thermal analysis (or DTA) is a thermo analytic technique, similar to differential scanning calorimetry. In DTA, the material under study and an inert reference are heated (or cooled) under identical conditions, while recording any temperature difference between sample and reference. This differential temperature is then plotted against time, or against temperature (DTA curve or thermo gram). Changes in the sample, either exothermic or endothermic, can be detected relative to the inert reference. Thus, a DTA curve provides data on the transformations that have occurred, such as glass transitions, crystallization, melting and sublimation. The area under a DTA peak denotes the enthalpy change and it is not affected by the heat capacity of the sample. Changes in the sample which lead to the absorption or evolution of heat can be detected relative to the inert reference. Differential temperatures can also arise between two inert samples when their response to the applied heat-treatment is not identical. DTA can therefore be used to study thermal properties and phase changes which do not lead to a change in enthalpy. The baseline of the DTA curve should then exhibit discontinuities at the transition temperatures and the slope of the curve at any point will depend on the micro structural constitution at that temperature.

A DTA apparatus consist of a sample holder comprising thermocouples, sample containers and a ceramic or metallic block; a furnace; a temperature programmer; and a recording system. The key feature is the existence of two thermocouples connected to a voltmeter. One thermocouple is placed in an inert material such as Al_2O_3, while the other is placed in a sample of the material under study. As the temperature is increased, there will be a brief deflection of the voltmeter if the sample is undergoing a phase transition. This occurs because the input of heat will raise the temperature of the inert substance, but be incorporated as latent heat in the material changing phase. A DTA curve can be used as a fingerprint for identification purposes.

Figure 3.7 DTA set up

CHAPTER-4

RESULTS & DISCUSSION

4.1 X-ray analysis:

The XRD pattern for the $MnZnFe_2O_4$ sample synthesized from pure chemicals for 2 hrs, 3 hrs and 4 hrs stirring time are given in Figure 4.1, 4.2 and 4.3 respectively.

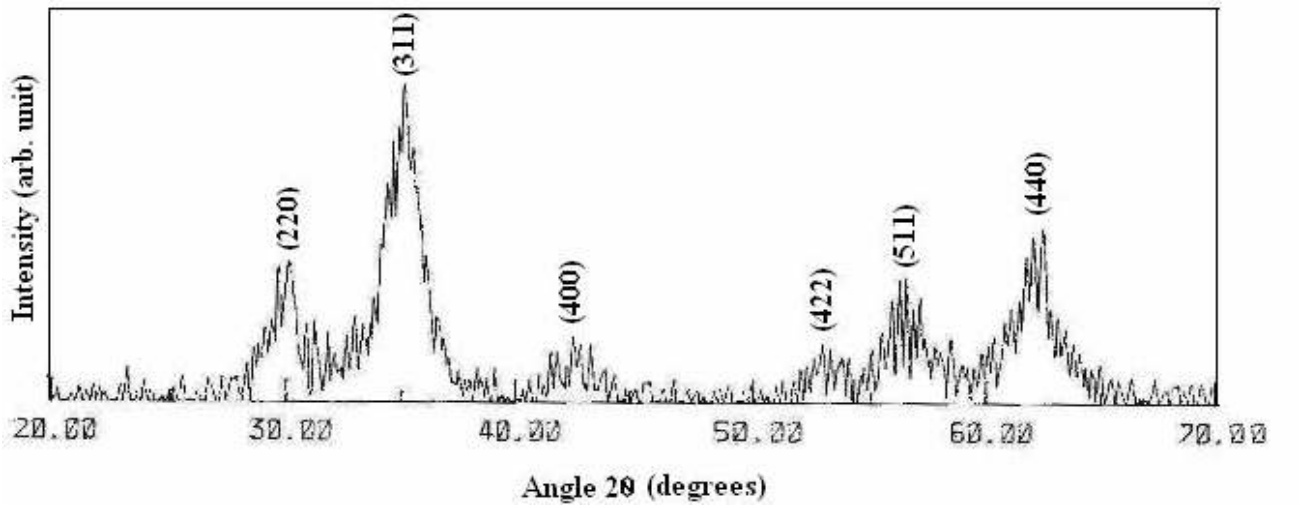

Figure 4.1 XRD pattern of the $MnZnFe_2O_4$ (From pure chemicals 2 hrs)

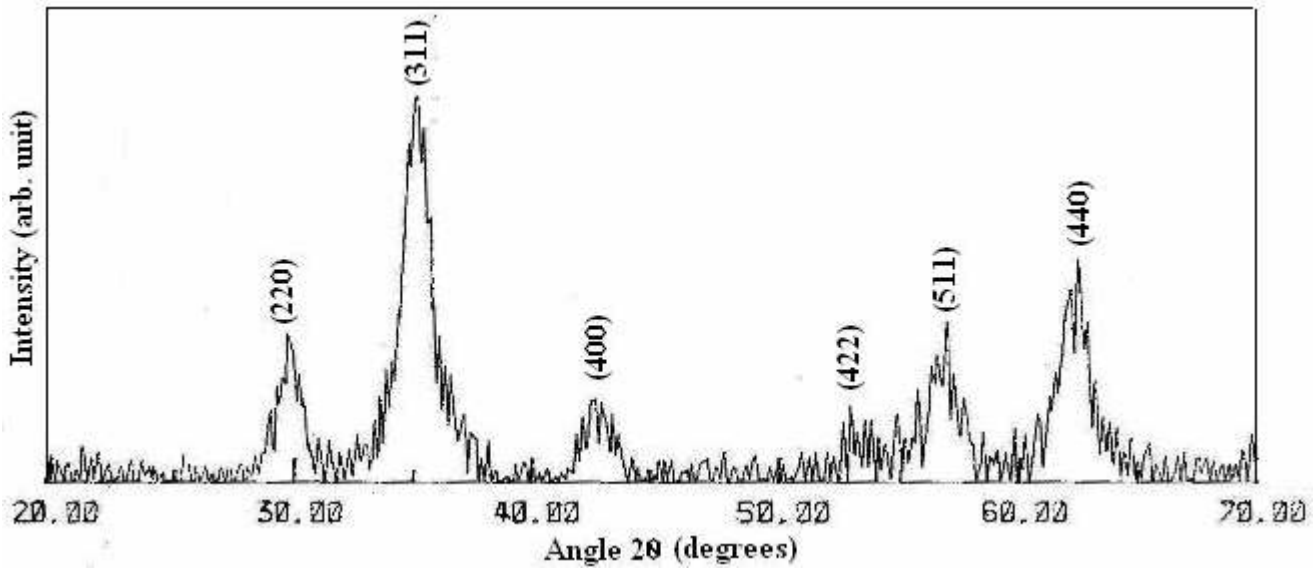

Figure 4.2 XRD pattern of the $MnZnFe_2O_4$ (From pure chemicals 3 hrs)

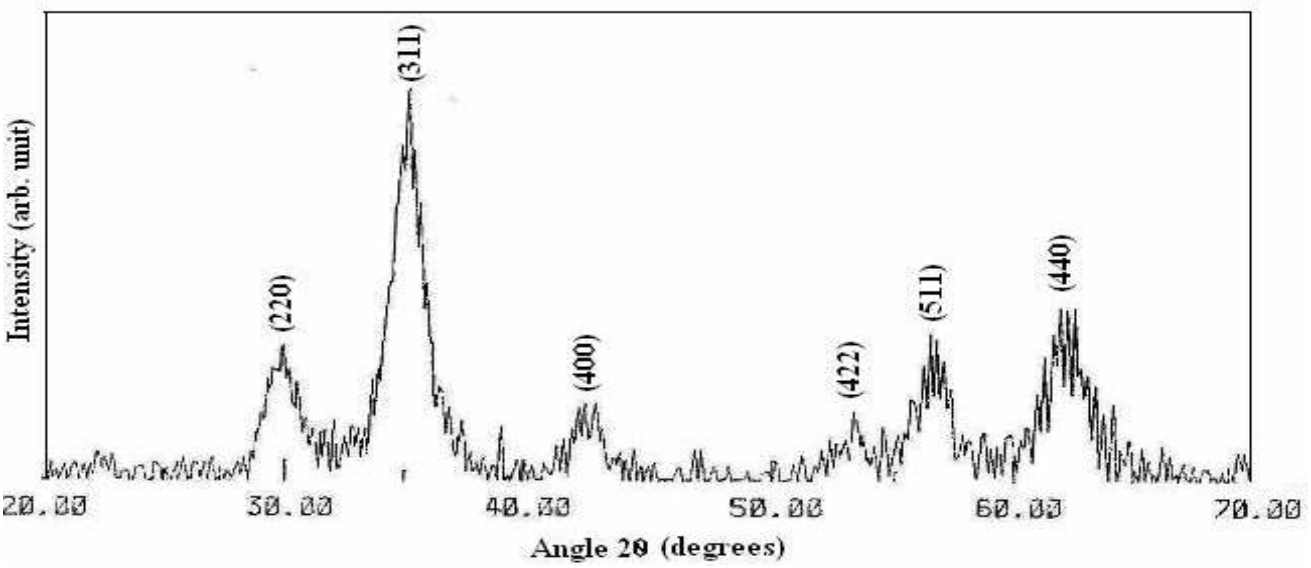

Figure 4.3 XRD pattern of the $MnZnFe_2O_4$ (From pure chemicals 4 hrs)

Each peak of the synthesized powders have been marked. It is evident from the X-ray peak that the compound synthesized is single phase Mn-Zn ferrite.

The XRD pattern for the $MnZnFe_2O_4$ compound synthesized from blue dust for 3 hrs stirring is given in Figure 4.4. Here also each peak has been marked. The results of X-ray analysis indicate that for the compound formed is single phase Mn-Zn ferrite.

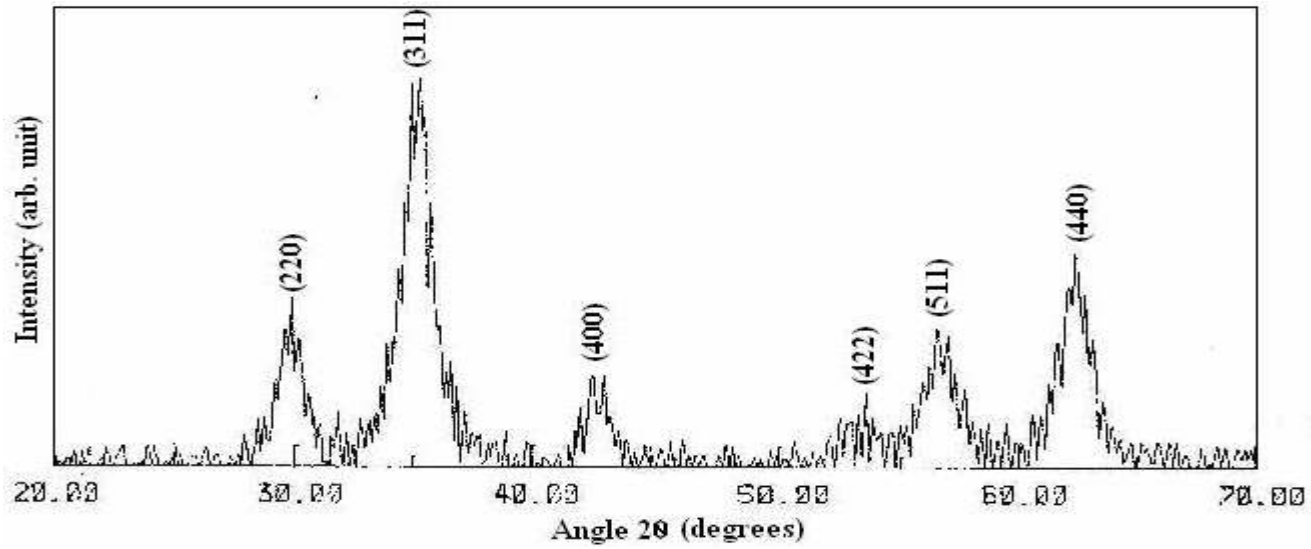

Figure 4.4 XRD pattern of the $MnZnFe_2O_4$ (From blue dust 3 hrs)

The analysis of X-ray diffraction pattern for $Mn_{0.5}Zn_{0.5}Fe_2O_4$ samples reveal a single phase cubic spinel structure with no other impurity phases for all the samples. The experimental peaks were matched with the theoretical generated one and no peak was found to be un-indexed. The lattice parameters were computed using the d values and the respective (h,k,l) parameters. The broad XRD lines indicate that the particles are of nanosize. The average particle size for the prepared powder has been calculated from broadening of XRD peaks using Debye-Scherrer formula

$$\mathbf{D=0.9\ \lambda/(w-w_1)\ \cos\theta}$$

Where D is the grain diameter, w and w_1 are the half-intensity width of the relevant diffraction peaks and the intrumental broadening respectively, λ is the X-ray wavelength and θ is the angle of diffraction.

The texture cofficients of the various planes for the samples synthesized from the pure chemicals and from the blue dust was also calculated. The texture cofficient for a given plane (hkl) can be calculated using the formula given below.

$$P(hkl) = \frac{I(hkl)}{I_0(hkl)}\left[\frac{1}{n}\sum_{i=1}^{n}\frac{I(hkl)}{I_0(hkl)}\right]^{-1}$$

Where n = No. of peaks

and I/I_0 is the intensity ratio for that peak

The results obtained from the XRD analysis including d values of the indexed peaks, particle size calculated from the indexed planes (D_{XRD}), lattice parameters and texture cofficients for each samples is given in the Table 4.1.

Table 4.1 Results obtained from the XRD analysis

S.No.	Sample	(hkl)	d(Å)	D_{XRD}(nm)	D_{averg}(nm)	a_0(nm)	Texture Cofficient
1.	**From Pure chemical 2 hrs**	(220)	2.959	4			0.849
		(311)	2.550	8			1.911
		(400)	2.113	8.5	**6.91**	**8.457**	0.676
		(422)	1.634	9			0.7529
		(511)	1.626	6			0.7722
		(440)	1.494	6			1.0425
2.	**From Pure chemical 3 hrs**	(220)	2.998	6			0.781
		(311)	2.539	8			1.840
		(400)	2.108	6	**7.33**	**8.421**	0.7435
		(422)	1.631	9			0.614
		(511)	1.614	9			0.856
		(440)	1.504	6			1.171

3.	**From Pure chemical 4 hrs**	(220)	2.978	4			0.740
		(311)	2.545	5			2.110
		(400)	2.106	6	**6.66**	**8.441**	0.634
		(422)	1.633	9			0.803
		(511)	1.612	7			0.761
		(440)	1.510	9			0.951
4.	**From Blue Dust 3hrs**	(220)	3.012	6			0.878
		(311)	2.539	8			2.041
		(400)	2.103	9	**6.83**	**8.421**	0.489
		(422)	1.640	9			0.735
		(511)	1.612	4			0.714
		(440)	1.511	5			1.143

The particle size for the samples synthesized by 2 hrs stirring is observed to vary from 4 nm to 9 nm and average particle size calculated for this sample was 6.91 nm. Similarly the particle size for the samples synthesized by 3 hrs and 4 hrs stirring was in the range from 6 nm to 9 nm and 4 nm to 9 nm respectively. The average particle size for these two samples was found to be 7.33

nm and 6.66 nm respectively. The particle size for the sample prepared from the blue dust was observed to vary from 4 nm to 9 nm and the average particle saize for this sample was 6.83 nm.

The lattice constants for the samples prepared from the pure chemicals for 2 hrs, 3 hrs and 4 hrs stirring was found to be 8.457 nm, 8.421 nm and 8.441 nm respectively. The lattice parameter for the sample prepared from blue dust was calculated and it was also found to be 8.421 nm. These results are in good agreement with the reported values**[19].**

The texture cofficients calculated for the samples synthesized from the pure chemicals and for blue dust show that all the planes are highly textured (oriented). The maximum texture cofficient for the samples synthesized from pure chemicals have been found for the planes (311) and (440). The same results were found for the samples prepared from the blue dust. These results confirm that the preferred direction of growth for the particles are along these planes in the case of pure chemicals as well as for blue dust. This confirms that the material synthesized from the blue dust has the same plane orientation as that for the pure chemicals.

4.2 DTA analysis:

The TG-DTA curves for the samples synthesized from the pure chemicals as well as blue dust have been studied for their thermal characterization. These are shown in the Figure 4.5 to 4.7. Similarly the for the powder synthesized from blue dust is also shown in Figure 4.8.

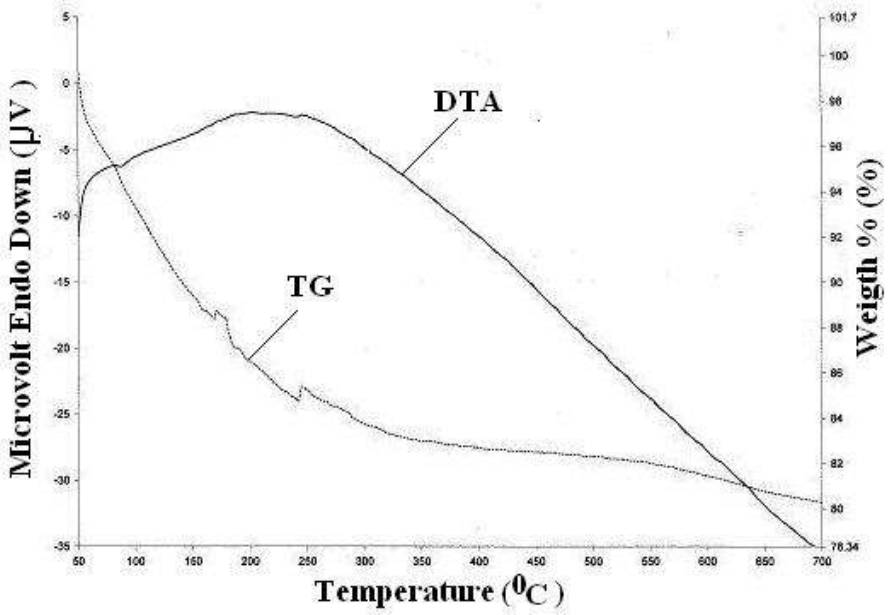

Figure 4.5 DTA curves for the $MnZnFe_2O_4$ (From pure chemicals 2 hrs)

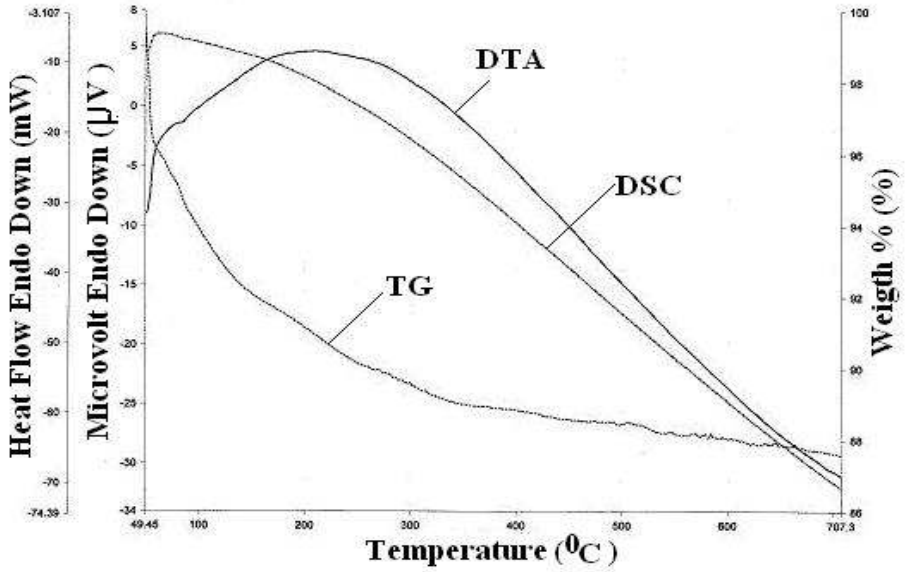

Figure 4.6 DTA curves for the $MnZnFe_2O_4$ (From pure chemicals 3 hrs)

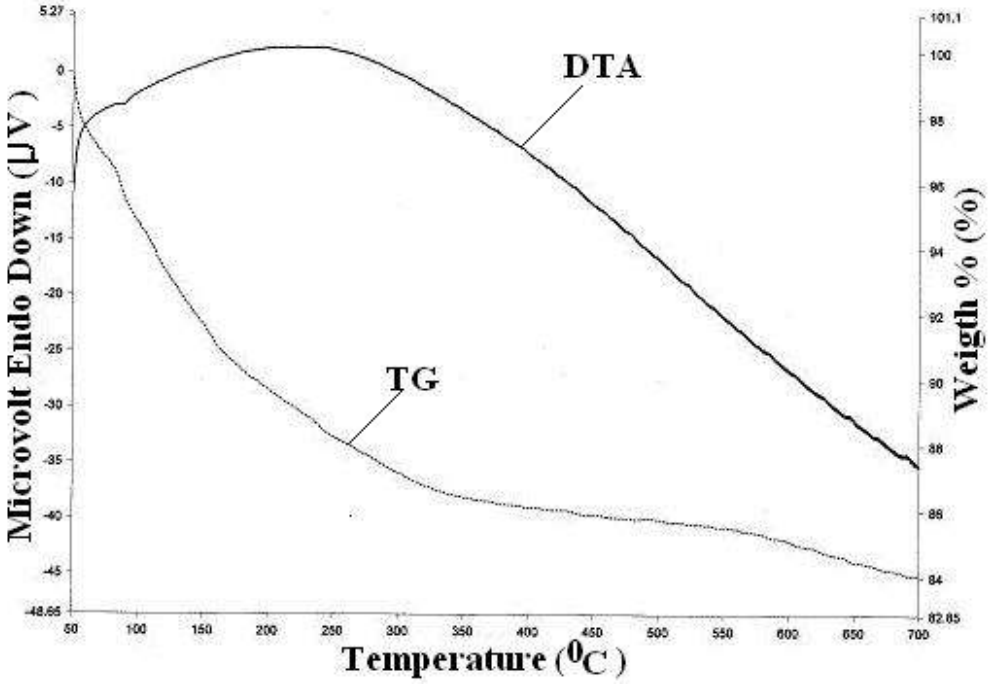

Figure 4.7 DTA curves for the $MnZnFe_2O_4$ (From pure chemicals 4 hrs)

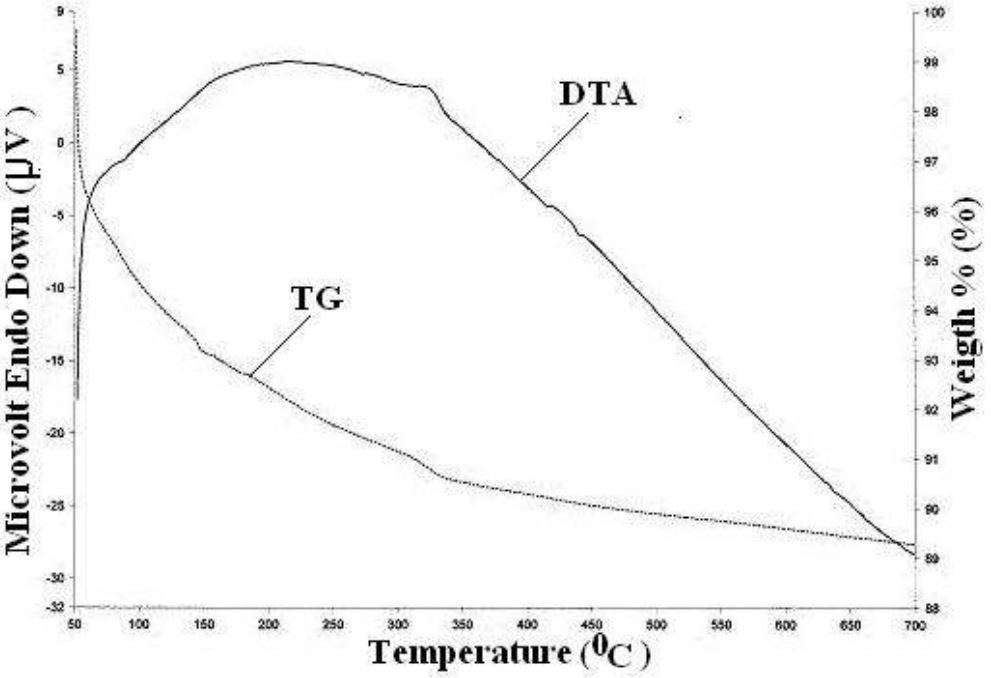

Figure 4.8 DTA curves for the $MnZnFe_2O_4$ (From blue dust 3 hrs)

The amount of water absorbed from the precipitated ferrite was estimated by the thermogravimetric analysis. TG-DTA curve were recorded simultaneously from 50°C to 700°C by a scan rate of 5^0 per min. in an inert atmosphere. The water content was estimated from the weight difference measured at 50°C and 700°C. The recorded weight losses with the increase in the temperature for the four samples is given in the Figure 4.5-4.8. The observed weigt loss is due to the desorption of the water from the samples. From the thermogravimetric analysis it is clear that in all the samples the maximum weight loss is taking place within 340°C. The absorbed water content was found to be maximum within this range and which varies from 11.5 wt% to 19.6 wt% for the samples. The weight loss estimated on further increse in temperature till 700°C was found to be only 1.5 wt%. Moreover, the thermal study has been done in the inert atmosphere . Hence, the entire weight loss within this range is only due to dehydration taking place**[19].** The estimated water content for the four samples is given in the Table 4.2 below:

Table 4.2 Estimated water content

S.NO.	**Sample**	**Estimated water content**
1.	**Pure chemical (2 hrs)**	19.6 wt%
2.	**Pure chemical (3 hrs)**	11.5 wt%
3.	**Pure chemical (4 hrs)**	16 wt%
4.	**Blue Dust**	10.6 wt%

The DTA analysis of the samples synthesized from pure chemicals shows nearly same behaviour. It shows a small peak around 80°C due to dehydration. The type of reaction and the temperature of the dehydration peak remain unaltered except the broad hump in the temperarure range 250°C-500°C. This may be due to the simultaneous sintering and growth of the ultrafine particles present. There is no other major peak observed in case of the samples synthesized from pure chemicals. This is an indication for completion of ferritization (formation of ferrites). Hence any further sintering or heat treatment is not required.

The DTA curve for the sample synthesizd from the blue dust shows some different behaviour than that of pure chemicals. The DTA curve for the blue dust sample shows one small exothermic and two small endothemic peaks in addition to the peak due to dehydration. The exothermic peak occurs at nearly 327°C and enothermic peaks occurs at nearly 418°C and 442°C. These peaks may due to change in oxidation state.

4.3 SEM analysis:

For microstructural analysis of the prepared samples was done by scanning electron microscopy (SEM). The SEM micrographs of the samples synthesized from the pure chemicals and blue dust are given below.

4.3.1 SEM for $MnZnFe_2O_4$

The SEM micrographs of the samples synthesized from the pure chemicals for three hrs stirring are given in Figure 4.9. The powders are spherical in shape.

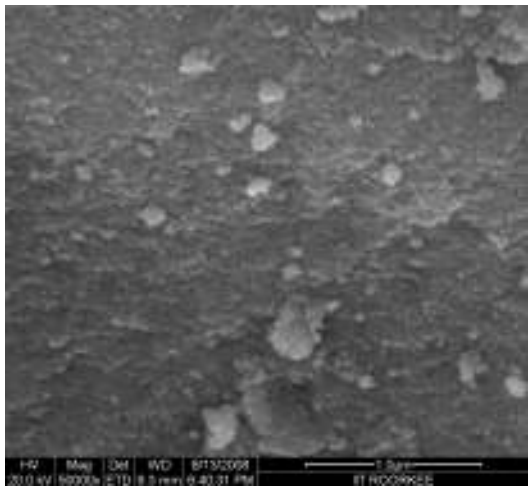

(a)Magnification=50000X

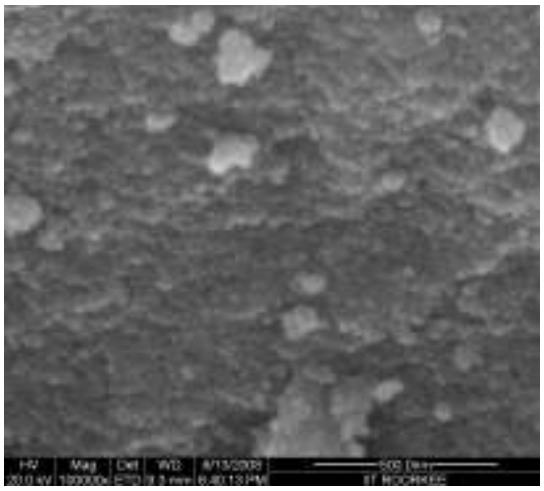

(b) Magnification=100000X

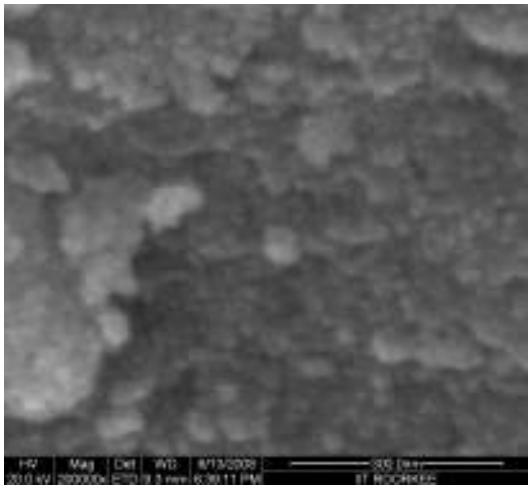

(c) Magnification=200000X

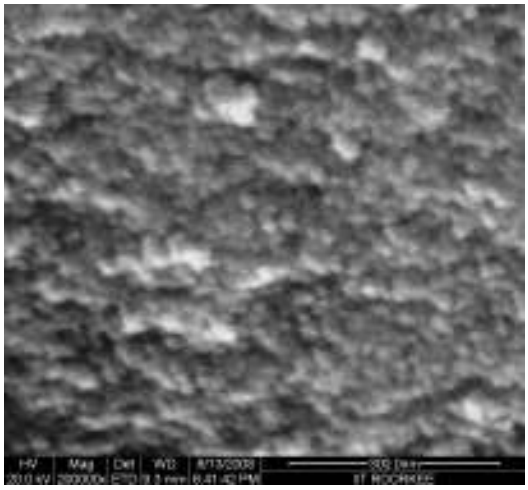

(d)Magnification=200000X

Figure 4.9 SEM micrographs for $MnZnFe_2O_4$ (From pure chemicals 3 hrs)

The SEM micrographs of the samples synthesized from the pure chemicals for four hrs stirring are given in Figure 4.10. Here also the powders are spherical in shape. However, clustering is observed. Since particles are nanosized so they try to cogulate and relaese its surface energy.

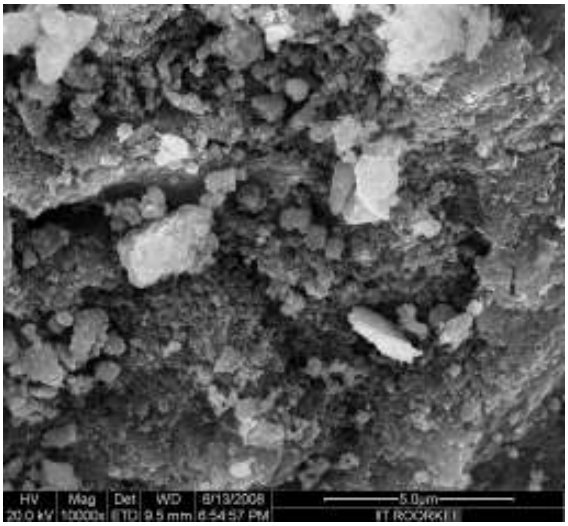

(a) Magnification=10000X

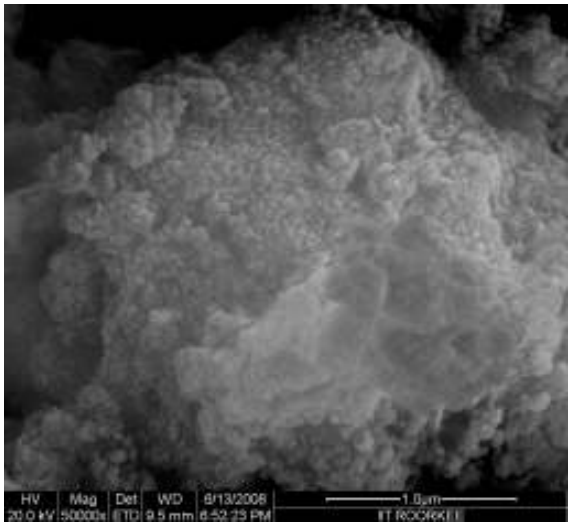

(b) Magnification=50000X

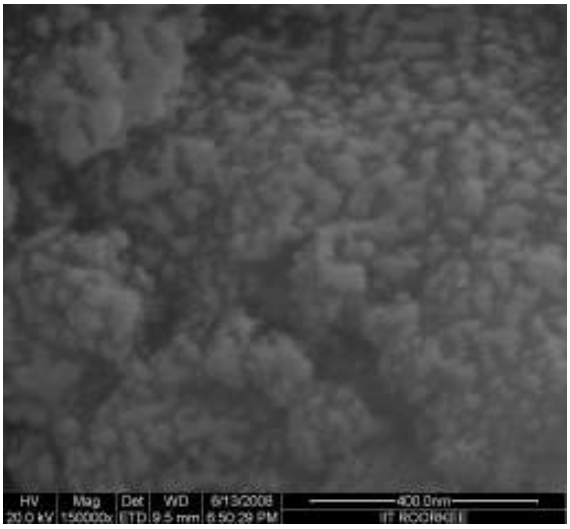

(c) Magnification=150000X

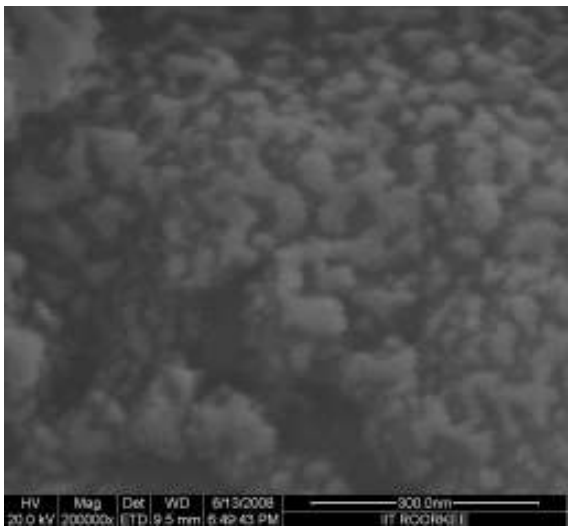

(d) Magnification=200000X

Figure 4.10 SEM micrographs for $MnZnFe_2O_4$ (From pure chemicals 4 hrs)

The SEM micrographs of the $MnZnFe_2O_4$ samples synthesized from the blue dust for three hrs stirring are given in Figure 4.11. The are spherical in nature and also of uniform size. Clustering is also observed in this case.

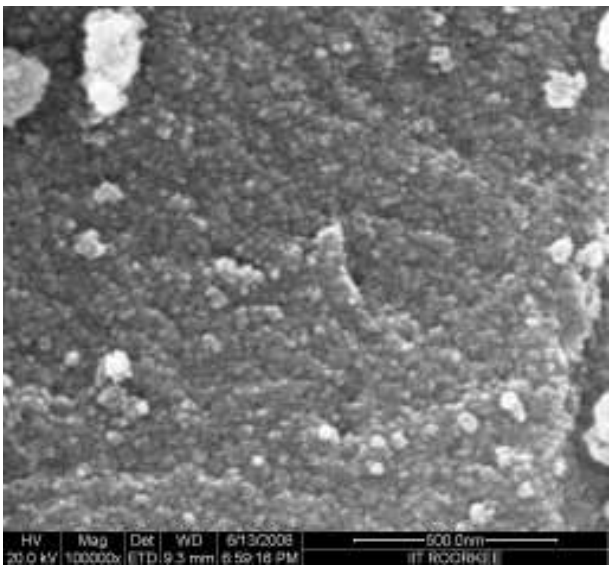

(a) Magnification=100000X

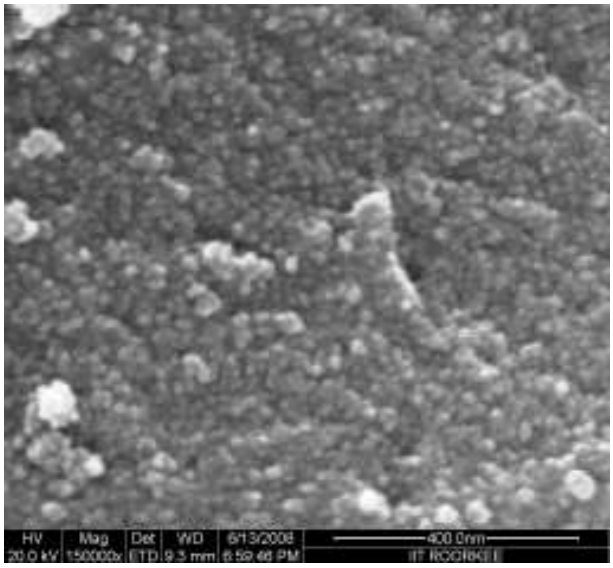

(b) Magnification=150000X

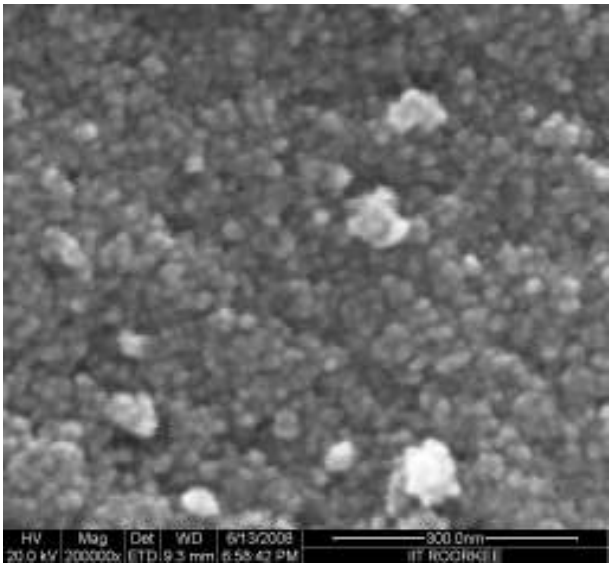

(c) Magnification=200000X

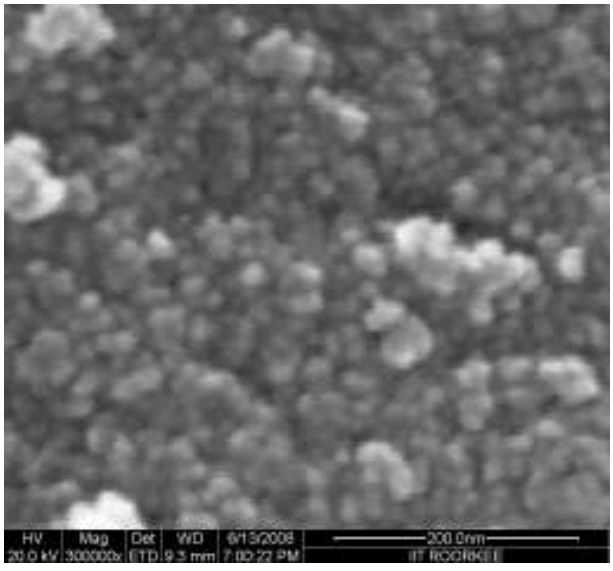

(d) Magnification=300000X

Figure 4.11 SEM micrographs for $MnZnFe_2O_4$ (From blue dust 3 hrs)

The SEM micrographs of the samples synthesized from pure chemicals and blue dust are given in the Figure 4.9 -4.11. The SEM for blue dust shows white coloured large ball shaped particle agglomerates poping out from a dark matrix. These white coloured agglomerates are also clearly visible in fig 4.9 and 4.10 for the pure chemicals. Higher magnification of this particular white agglomerate shows individual fine particles as can be seen in Figure 4.10(b).

4.4 EDS analysis:

4.4.1 EDS for $MnZnFe_2O_4$

The EDS pattern for the $MnZnFe_2O_4$ sample synthesized from pure chemical for three hrs stirring are given in Figure 4.12.

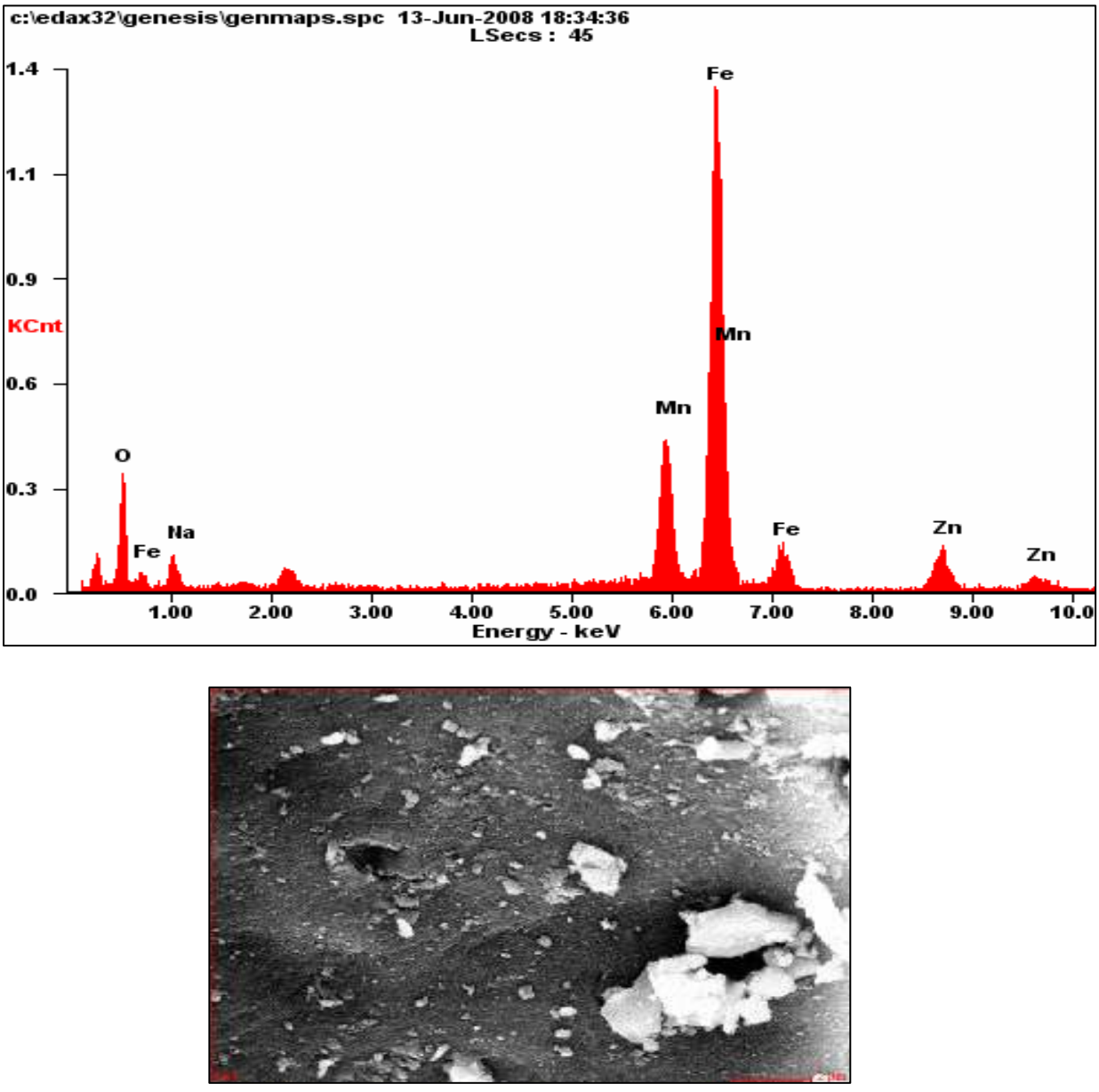

Figure 4.12 EDS pattern for $MnZnFe_2O_4$ (From pure chemicals 3 hrs)

Apart from Fe, Mn, Zn and O peaks the EDS analysis shows the presence of Na peaks. The presence of Na indicate that the sample requires more washing to remove Na ions.

The EDS pattern for the $MnZnFe_2O_4$ sample synthesized from pure chemical for four hrs stirring are given in Figure 4.13.

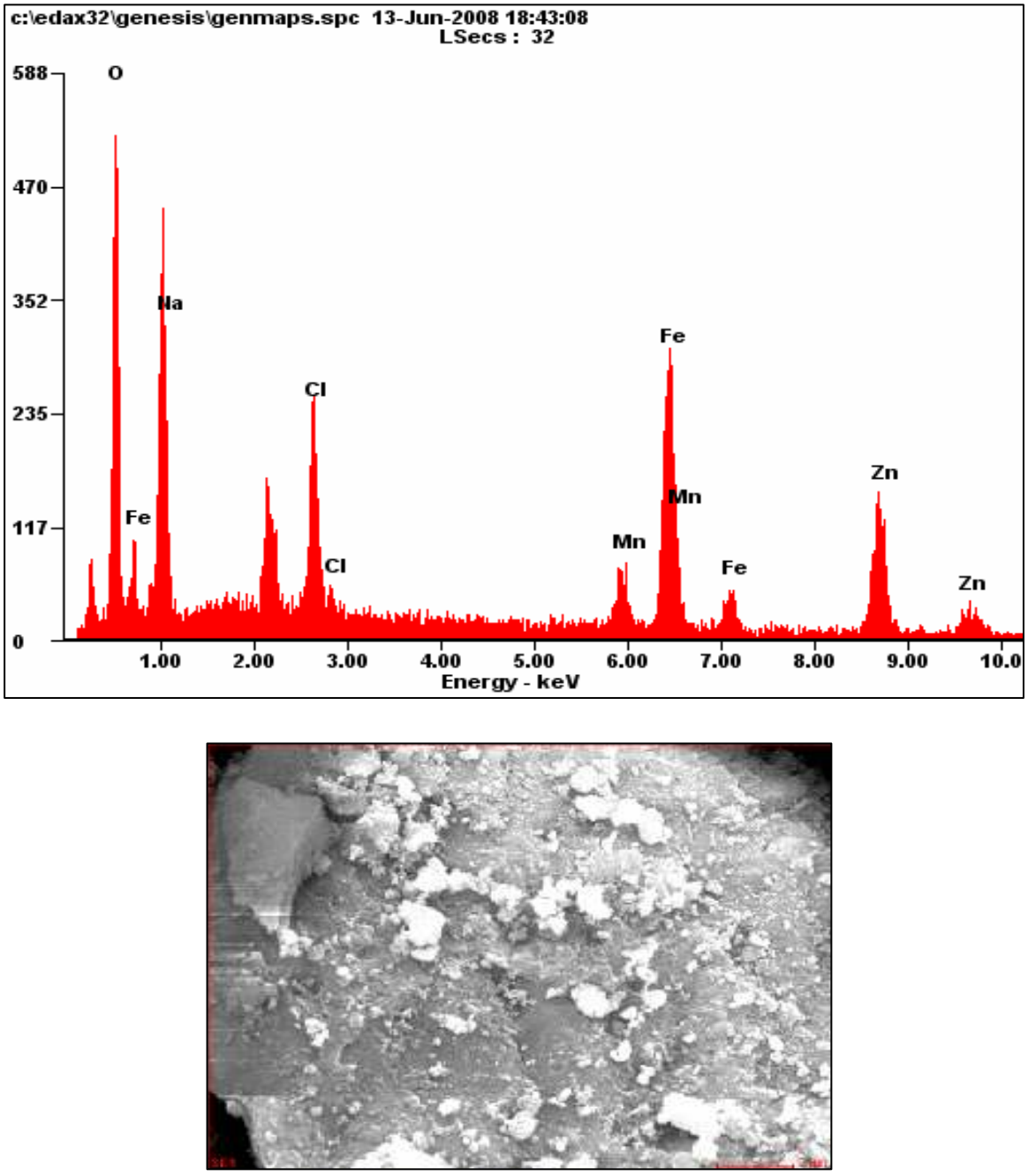

Figure 4.13 EDS pattern for $MnZnFe_2O_4$ (From pure chemicals 4 hrs)

Here also NaCl remain in solution which could not be washed out. The sample requires more washing.

The EDS pattern for the $MnZnFe_2O_4$ sample synthesized from blue dust for three hrs stirring are given in Figure 4.14.

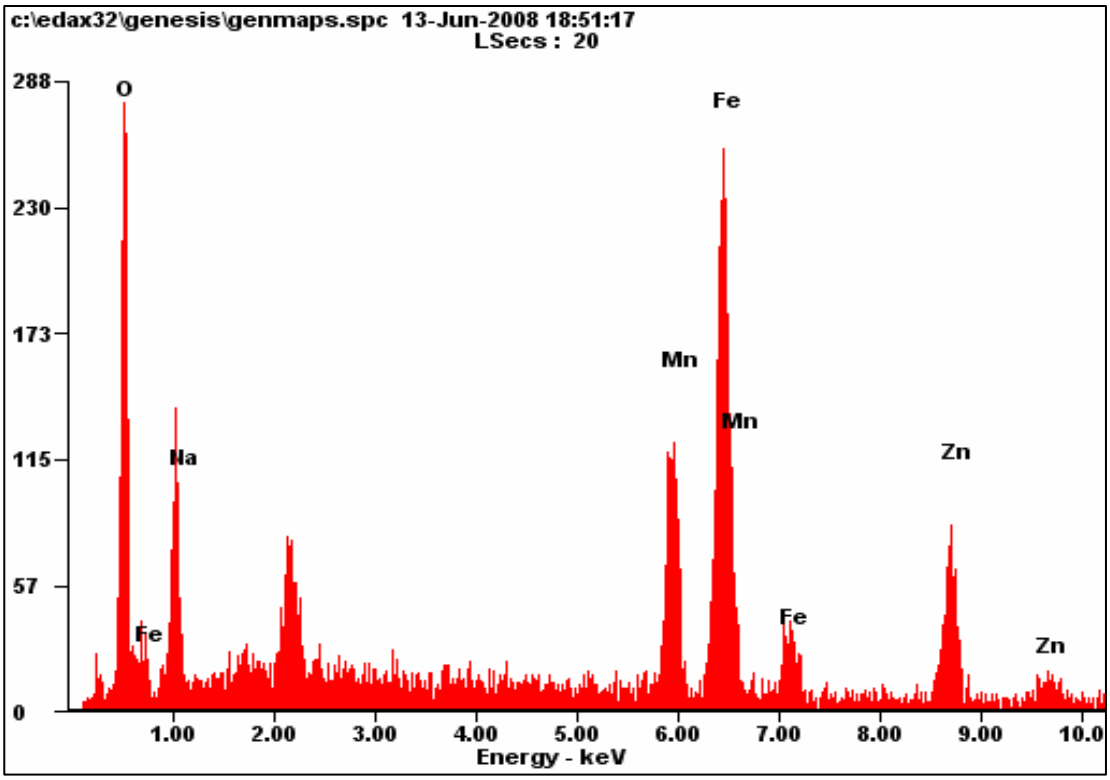

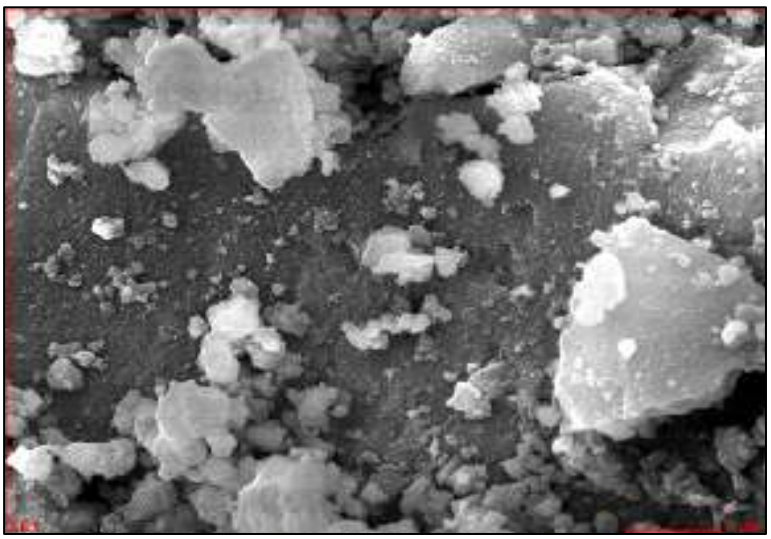

Figure 4.14 EDS pattern for $MnZnFe_2O_4$ (From blue dust 3 hrs)

In this sample we observe that Na remains in solute and could not be washed out. Since we have used cold distilled water in which dissolution of NaCl has not taken place so the presence of this peak is obvious.

4.5 EDS Results:

In order to estimate the compostion of the samples and their percentage in the samples the energy dispersive spectroscopy has been done. The results of the EDS analysis for the samples synthesized from pure chemical for 3 hrs and 4 hrs stirring time and sample synthesized from blue dust are given below:

4.5.1 EDS Results for $MnZnFe_2O_4$

The EDS result for the sample synthesized from the pure chemical for 3 hrs stirrirng is given in the Table 4.3.

Table 4.3 EDS result for Pure Chemical (3hrs)

Element	Wt%	At%
O	05.72	17.04
Na	03.25	06.73
Mn	16.07	13.93
Fe	61.81	52.72
Zn	13.15	09.58

The EDS result for the sample synthesized from the pure chemical for 4 hrs stirrirng is given in the Table 4.4.

Table 4.4 EDS result for Pure Chemical (4hrs)

Element	Wt%	At%
O	20.17	40.25
Na	18.02	25.02
Cl	05.15	04.64
Mn	04.69	02.73

Fe	23.77	13.59
Zn	28.21	13.78

The EDS result for the sample synthesized from the blue dust for 3 hrs stirrirng is given in the Table 4.5.

Table 4.5 EDS result for Blue Dust(3hrs)

Element	Wt%	At%
O	16.35	37.43
Na	10.63	16.93
Mn	14.09	09.40
Fe	33.76	22.14
Zn	25.18	14.11

The EDS results shows that as we are increasing the time of stirring the percentage of the oxygen and zinc are increasing while the percentage of manganese and iron are decreasing. Also EDS results shows that in addition to required elements the elements like sodium and chlorine are also present in the materials. This may be due to presence of unwanted sodium chloride in the sample which can not be removed at the time of the washing.

4.6 TEM analysis: For the determination of particle size and their morphology the TEM analysis of the samples prepared from the pure chemicals and bule dust has been done.

4.6.1 TEM for $MnZnFe_2O_4$

TEM micrograph of $MnZnFe_2O_4$ compound synthesized from pure chemicals for three hours stirring are given in Figure 4.15.

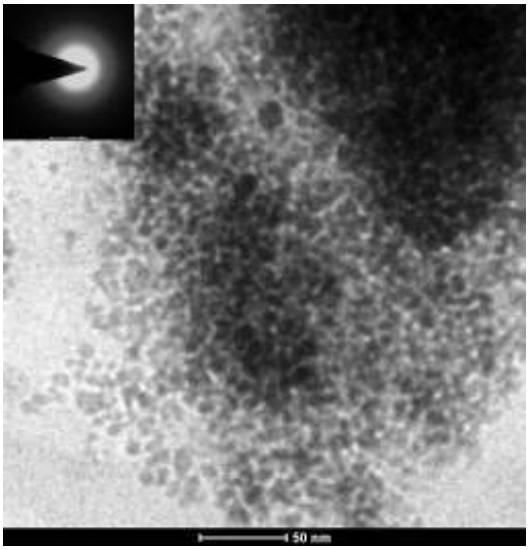

(a)

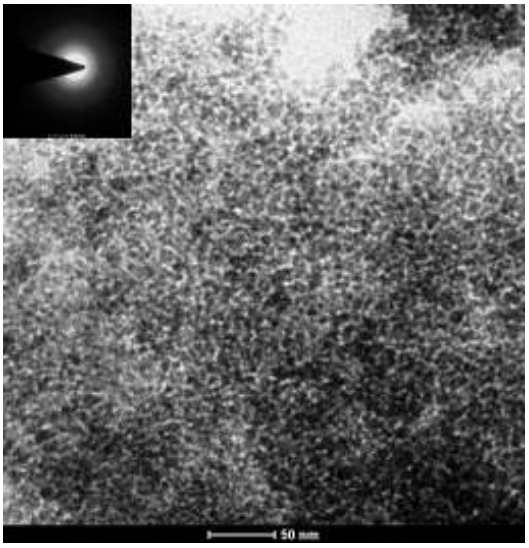

(b)

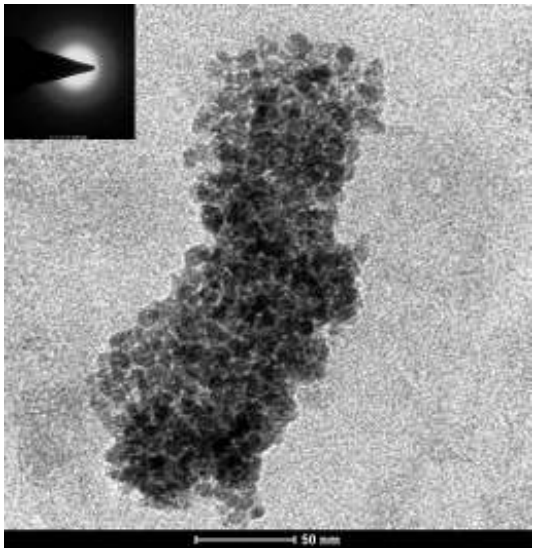

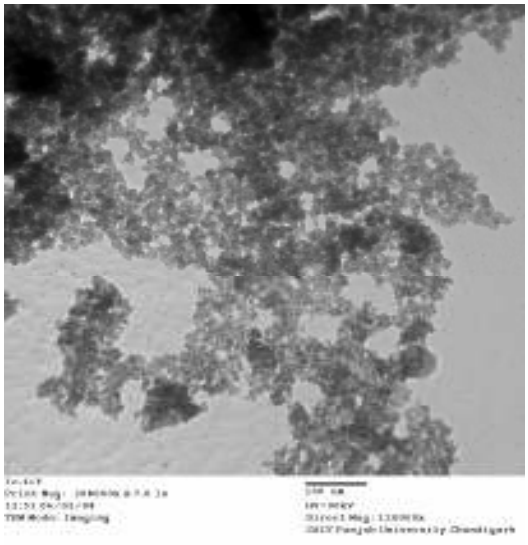

(c) **(d)**

Figure 4.15 TEM micrograph for $MnZnFe_2O_4$ (From pure chemicals 3 hrs)

TEM micrograph of $MnZnFe_2O_4$ synthesized from the pure chemicals for four hours stirring are given in Figure 4.16.

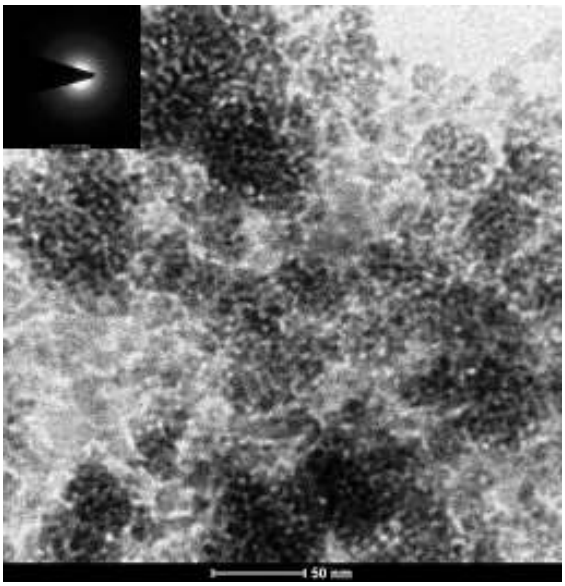

(a)

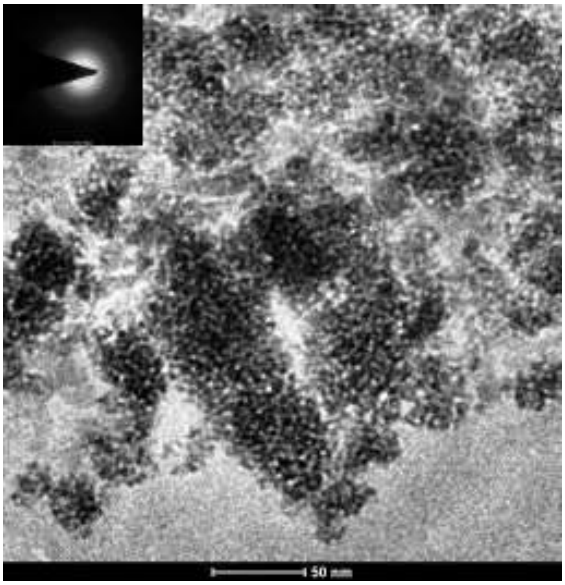

(b)

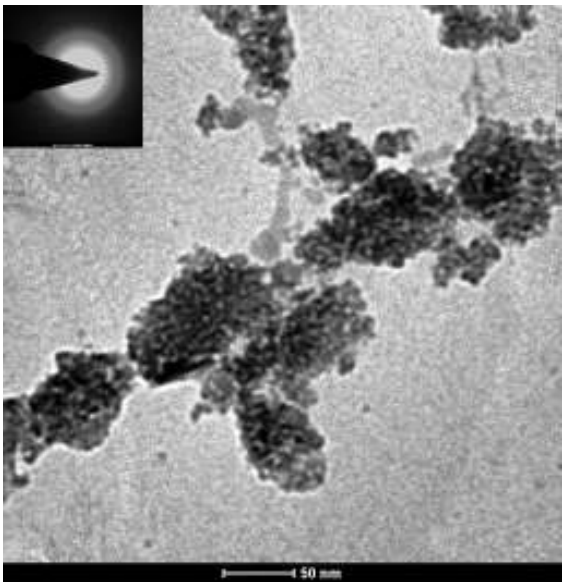

(c)

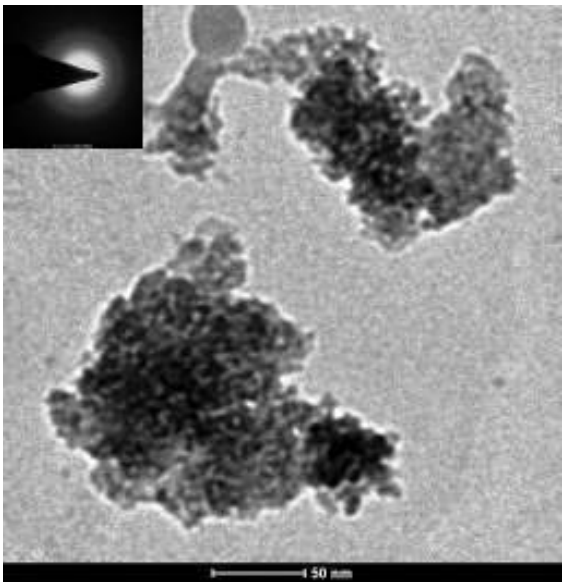

(d)

Figure 4.16 TEM micrograph for $MnZnFe_2O_4$ (From pure chemicals 4 hrs)

TEM micrographs of $MnZnFe_2O_4$ powder synthesized from blue dust for three hours stirring are given in Figure 4.17.

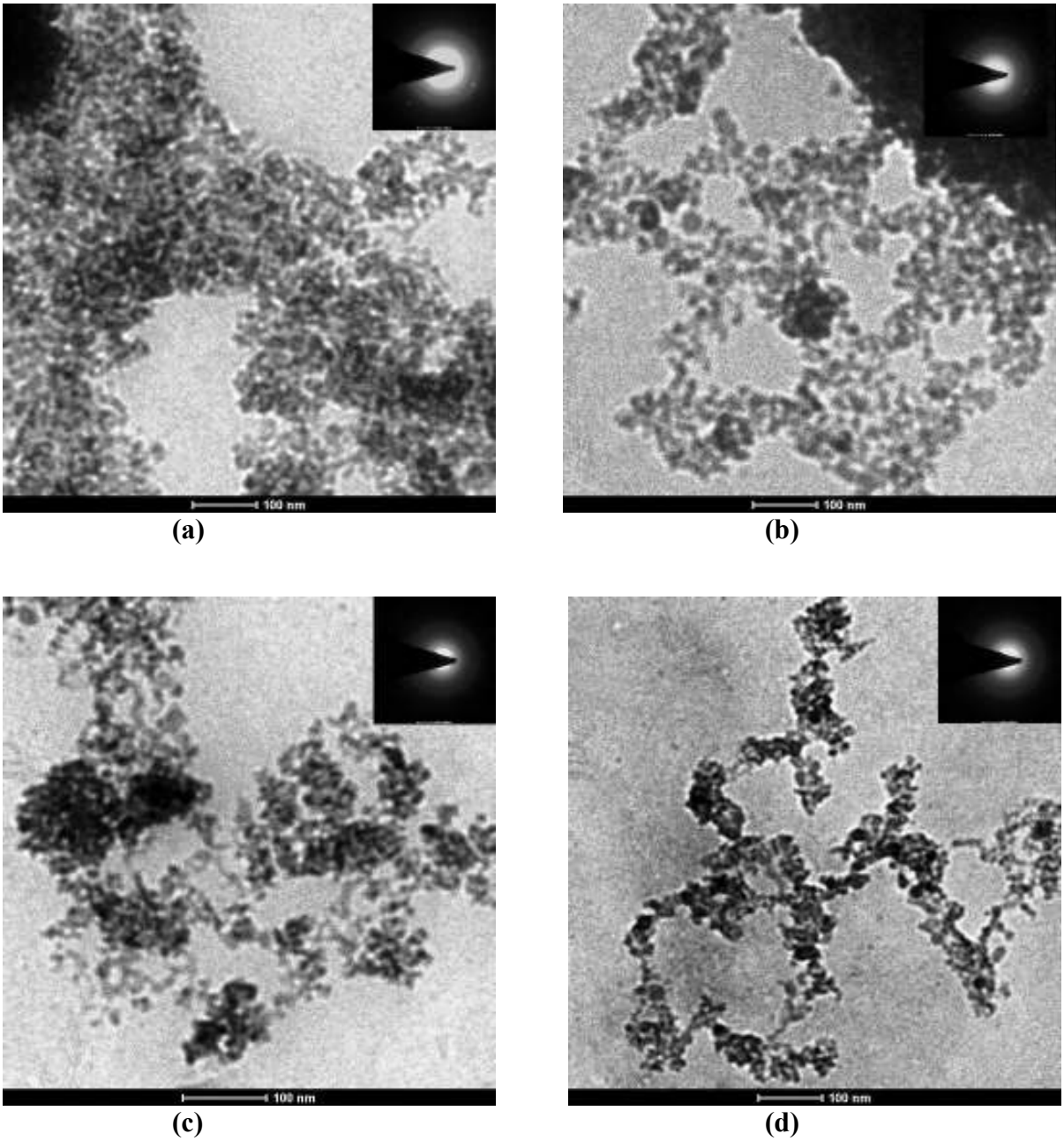

(a) **(b)**

(c) **(d)**

Figure 4.17 TEM micrograph for $MnZnFe_2O_4$ (From Blue Dust 3 hrs)

A typical bright-field TEM image of the $MnZnFe_2O_4$ samples synthesized from 3 hrs and 4 hrs stirring and also for the blue dust are given in the Figure 4.15 -4.17. The direct observations of the lattice image reveal that the particles are approximately spherical in shape. The TEM images also reveal that particles are agglomerated. The same results about the morphology and the agglomeration are obtained by the SEM analysis. Hence TEM images are in the good agreement with the SEM images. Because of the smaller particle size (single domain) particles experience a permanent magnetic moment proportional to their volume. Hence each particle is permanently magnetized and gets agglomerated. The average particles size calculated from the different regions of the image is in good agreement with that calculated from the X-ray analysis. The selected area electron diffraction (SAED) pattern of the samples are also given along with the TEM images. The selected area diffraction pattern of the sample made from the blue dust shows rings made up of discrete spots, indicating high crystallinity, the rings are consistent with the cubic spinel structure with an intense ring pattern form (hkl) plane. No secondary phases are found. The observed selected area electron diffraction pattern are also consistent with the results that obtained from the X-ray analysis**[17].** Some TEM images also show the agglomeration of the particles.

CHAPTER-5

CONCLUSIONS AND FUTURE SCOPE OF THE WORK

5.1 Conclusions:

From the work done for the synthesis of Mn-Zn nano-ferrite following conclusions can be drawn:

1. Chemical coprecipitation method is a very good method for the synthesis of the Mn-Zn ferrite where uniform size of the particle can be achieved by suitably controlling the pH and temperatur of the solution. $MnZnFe_2O_4$ nanoparticles have been successfully synthesized by chemical coprecipitation method.

2. The stirring time does not make a great impact on the synthesis of $MnZnFe_2O_4$ nanoparticles within the time range during which the experiments were performed. The particles size, lattice constant and other parameters are nearly same for the samples synthesized from the pure chemicals for 2 hrs, 3hrs and 4 hrs stirring.

3. The synthesis of $MnZnFe_2O_4$ nanoparticles has been done by two different types of starting materials i.e. from the pure chemicals and from the waste iron ore blue dust. In both the cases the particle size is nearly same and very fine. The particle size was found to be nearly 4-9 nm.

4. The results obtained from the blue dust are similar to that of the pure chemicals i.e. $MnZnFe_2O_4$ materials synthesized from blue dust have nearly same particle size and lattice parameter as that from the pure chemical. Hence the results confirm that waste material blue dust can be utilised for the production of the Mn-Zn ferrite material. This can result in the cost reduction as well as utilization of the waste material blue dust.

5.2 Future Scope of the work:

There are number of motivations for synthesis and characterization of manganese-zinc ferrites, better understanding of co-precipitation process, a close control on the synthesis parameters can result in more efficient ferrites. Control of particle size in the nanometer range by the variation of synthesis condition gives much better properties than traditional bulk. The study of optimum conditions for the ferrite powder synthesis can also minimize the cost of the materials. It is suggested that other processing parameters like temperature, pH should be optimised to achieve very fine size powder. Moreover, the magnetic properties of the synthesized powder should be measured to finds its end applications.

REFERENCES:

1). Chikazumi, S. 1964. Physics of Magnetism, New York: john Wiley & sons.

2). S.H. Chen, S.C. Chang . IEEE Trans on. Mag., Vol. 28, no. 5, Sep. 1992.

3). Skolyszewska et al. synthesized Materials Science and Engineering B 118 (2005) 84–86

4). R. Arulmurugan et. al Journal of Magnetism and Magnetic Materials 288 (2005) 470-477

5). A. K. Singh et. al Materials Letters 57 (2003) 1040– 1044

6). Ming Ma, et. al Colloids and Surfaces A: Physicochem. Eng. Aspects 224 (2003) 207-212

7). Dong Limin Journal of Rare Earths, Vo1.24, Spec. Issue, Dec. 2006, p .54

8). M. Mozaffari, et. al Journal of Alloys and Compounds xxx (2007) xxx–xxx

9). I. P. Kilbride and R. Freer IEEE Trans on. Mag., Vol. 36, No. 1, Jan. 2000

10). Setsuo Yamamoto . Journal of Magnetism and Magnetic Materials 2001.

11). S.H. Keluskar et al. Journal of Magnetism and Magnetic Materials December 2005.

12). Nobuyuki Kikukawa, et. al Journal of Magnetism and Magnetic Materials Volume 284, December 2004, Pages 206-214

13). R. Justin Joseyphus et.al Journal of Physics and Chemistry of Solids Volume 67, Issue 7, July 2006, Pages 1510-1517

14). Wang Xin,Rare Metals, Vol.25, Spec. Issue, October 2006, p.526.

15). Goldman et al. United state patents 14 June 1978

16). B. Parvatheeswara Rao, et. al IEEE Transactions on Magnetics, Vol.42, No. 10, October 2006.

17). Kinnari Parekh, et. al, Nanotechnology 17 (2006) 5970–5975

18). S. Otobe, et. al, IEEE Transactions on Magnetics, Vol 35, No. 5, September 1999.

19). R. Arulmurugan, G.Vaidyanathan et. al, Journal of Magnetism and Magnetic Materials, 298 (2006), 83-94.